Lappeenranta
University of Technology

M.Sc. Jani Heikkinen

VIRTUAL TECHNOLOGY AND HAPTIC INTERFACE SOLUTIONS FOR DESIGN AND CONTROL OF MOBILE WORKING MACHINES

Thesis for the degree of Doctor of Science (Technology) to be presented with
due permission for public examination and criticism in the Auditorium 1382
at Lappeenranta University of Technology, Lappeenranta, Finland on the 30th
of August, 2013, at noon.

Acta Universitatis
Lappeenrantaensis 525

Supervisor Professor Heikki Handroos
Department of Mechanical Technology
Faculty of Technology
Lappeenranta University of Technology
Finland

Reviewers Professor Asko Ellman
Department of Engineering Design
Tampere University of Technology
Finland

TkT Hassan Yousefi
Konnexio Inc.
London
Canada

Opponents Professor Asko Ellman
Department of Engineering Design
Tampere University of Technology
Finland

TkT Hassan Yousefi
Konnexio Inc.
London
Canada

ISBN 978-952-265-441-0
ISBN 978-952-265-442-7 (PDF)
ISSN-L 1456-4491
ISSN 1456-4491
Lappeenrannan teknillinen yliopisto
Yliopistopaino 2013

Abstract

Jani Heikkinen

VIRTUAL TECHNOLOGY AND HAPTIC INTERFACE SOLUTIONS FOR DESIGN AND CONTROL OF MOBILE WORKING MACHINES

Commercially available haptic interfaces are usable for many purposes. However, as generic devices they are not the most suitable for the control of heavy duty mobile working machines like mining machines, container handling equipment and excavators. Alternative mechanical constructions for a haptic controller are presented and analysed. A virtual reality environment (VRE) was built to test the proposed haptic controller mechanisms. Verification of an electric motor emulating a hydraulic pump in the electro-hydraulic system of a mobile working machine is carried out. A real-time simulator using multi-body-dynamics based software with hardware-in-loop (HIL) setup was used for the tests. Recommendations for further development of a haptic controller and emulator electric motor are given.

Lappeenranta 2013
88 pages
Acta Universitatis Lappeenrantaensis 525
Diss. Lappeenranta University of Technology
ISBN 978-952-265-441-0, ISBN 978-952-265-442-7 (PDF)
ISSN-L 1456-4491
ISSN 1456-4491

Keywords: 3D, drives, force feedback, haptics, hardware-in-the-loop (HIL), human machine interface (HMI), mobile machine, model, permanent magnet machine, pump, real-time simulation, real-time simulator, teleoperation, virtual reality (VR)

UDC 004.94:004.946:004.383.4:621.22:681.5

Acknowledgements

The research work has been carried out during the years 2009 – 2013 in the Laboratory of Intelligent Machines, Department of Mechanical Engineering, Lappeenranta University of Technology. The research was enabled by the financial support of Tekes, the Finnish Funding Agency for Technology and Innovation and FIMECC Oy (Finnish Metals and Engineering Competence Cluster).

I would like to express my gratitude to my supervisor Professor Heikki Handroos for good innovative guiding and endless support during my work. I would like to also thank Professor Huapeng Wu for his willingness to help me whenever I needed it.

I wish to thank the pre-examinators Professor Asko Ellman and Dr Hassan Yousefi for their valuable comments to improve the manuscript.

My special thanks to my co-workers Juha Koivisto and Lauri Luostarinen for help in all kinds of construction and prototyping problems.

The valuable help of the staff of Laboratory of Intelligent Machines and the Department of Mechanical Engineering is also appreciated. Thank you for Professor Juha Pyrhönen and Department of Electrical engineering for help in the hydraulics emulation project. The support of the researchers of the Laboratory of Virtual Technology, Tampere University of Technology in selecting components and systems for the simulator laboratory is kindly acknowledged.

I would like to thank my friends for helping me survive through my studies and especially express gratitude to my dear wife Tatiana Minav and to my parents for always supporting me.

Heikkinen Jani
April 2013
Lappeenranta, Finland

Dedicated

To the memory of my grandparents.

Contents

List of publications

This thesis contains material from the following papers. The rights have been granted by publishers to include the material in dissertation.

I. Heikkinen, J., and Handroos, H. (2013). Design of a Human Machine Interface for a Mobile Machine using Simulation in Virtual Reality Environment. *International Review on Modelling and Simulations (IREMOS)*, Vol.6, N.1.

II. Heikkinen J., Minav, T., Handroos, H., and Pyrhönen, J. (2012). Real-time HIL-simulation for testing of electric motor drives emulating hydraulic systems. *International Review of Electrical Engineering (IREE)*, Vol.7, N.6.

III. Heikkinen, J., and Handroos, H. (2013). Haptic Controller for Mobile Machine Teleoperation. *International Review of Automatic Control (IREACO)*, Vol. 6 N.3.

IV. Heikkinen, J., Luostarinen, L., and Handroos, H. (2012). Virtual environment for investigating Human Machine Interface in Machines with hydraulic transmissions. *Proceedings of the 7th FPNI PhD Symposium on Fluid Power*, Reggio Emilia, Italy, June 27-30, 2012, pp. 225-234.

The author of this thesis is the main author of the papers listed above and gave the presentation in the 7th FPNI PhD Symposium on Fluid Power in Italy 2012.

Nomenclature

Latin alphabets

A_{cyl}	cross-section area of the hydraulic cylinder	m^2
a_i	Denavit-Hartenberg parameter	
a_{i-1}	Modified Denavit-Hartenberg parameter	
B_e	bulk modulus of the system	Pa
b_m	viscous friction coefficient	Nms/rad
C	spring constant of shaft	Nm/rad
d_i	Denavit-Hartenberg parameter	
D_{mshaft}	diameter of motor shaft	m
D_p	hydraulic pump displacement	m^3/rad
F_{piston}	force of the cylinder piston	N
$f_{refresh}$	digital signal frequency	Hz
G	shear modulus of steel	Pa
I	electrical current	A
J_{mrotor}	inertia moment of rotor	kgm^2
K_e	voltage constant	Vs/rad
K_m	torque constant	Nm/A
L	distance between two joints	m
L_{coil}	coil inductance	H
L_{mshaft}	length of the shaft	m
p	hydraulic pressure	Pa
pos_{ctrl}	controller position signal	m
pos_{cur}	current absolute position of the joint	pulses
pos_{zero}	absolute position of the axis at zero reference point	pulses
Q_{cyl}	hydraulic cylinder's flow rate	m^3/s
Q_{epump}	flow rate of emulated pump	m^3/s
Q_{pump}	flow rate of the hydraulic pump	m^3/s
R_a	coil resistance	Ω
Radstep	amount of radians per increment of one servo position step	rad
T_{em}	torque of electric motor	Nm
T_{out}	load torque	Nm
T_{pump}	torque on the hydraulic pump shaft	Nm
$T_{settling}$	settling time	s
U	supply voltage	V
V_t	total volume of the hydraulic cylinder and tube	m^3
x_{cyl}	position of the cylinder piston	m

Greek alphabets

α_i	Denavit-Hartenberg parameter
α_{i-1}	Modified Denavit-Hartenberg parameter

Δp	pressure difference across hydraulic pump	Pa
η_{HM}	hydro-mechanical pump efficiency	
η_{vol}	volumetric pump efficiency	
θ	rotor angle	rad
θ_1	angle of joint	rad
θ_2	angle of joint	rad
θ_3	angle of joint	rad
τ_f	electrical time constant of a motor	s
τ_m	mechanical time constant of a motor	s
τ_{m1}	mechanical time constant	s
τ_{m2}	mechanical time constant	s
ω_{act}	actual speed of the emulator electric motor	rad/s
ω_{shaft}	angular speed of shaft	rad/s
ω_{epump}	emulated pump speed	rad/s

Abbreviations

3D	Three Dimensional
A/D	Analog to Digital
CPU	Central Processing Unit
DOF	Degrees Of Freedom
EFFIMA	Energy and life cycle cost effective machines
EMF	Electromotive Force
FIMECC	Finnish Metals and Engineering Competence Cluster
GPU	Graphics Processing Unit
HIL	Hardware-In-the-Loop
HMI	Human Machine Interface
I/O	Input/Output
IR	InfraRed
LEFA	New generation Human-Centered Design Simulators for Life Cycle Efficient Mobile Machines
LUT	Lappeenranta University of Technology
MFC	Microsoft Foundation Class libraries
PC	Personal Computer
PS/2	IBM Personal System/2
R&D	Research and Development
rpm	Rotations Per Minute
RTG	Rubber Tyred Gantry
TCP	Transmission Control Protocol
UDP	User Datagram Protocol
UI	User Interface
USB	Universal Serial Bus

VR	Virtual Reality
VRE	Virtual Reality Environment
VRERS	Virtual Reality Environment and Real-time Simulator
VRPN	Virtual Reality Peripheral Network

1 Introduction

1.1 Background

This research was conducted in the Energy and Life Cycle Cost Efficient Machines (EFFIMA) research program, project New Generation Human-Centered Design Simulators for Life Cycle Efficient Mobile Machines (LEFA), managed by the Finnish Metals and Engineering Competence Cluster (FIMECC), with the aim of developing and designing a virtual reality (VR) based tool for the purpose of mobile machine design, testing and driver training.

Virtual reality environments and real-time simulators (VRERS) have evolved to be a useful design and analysis tool at an early stage in the design for evaluating performance of human operated mobile working machines (Viitaniemi, Aromaa, Leino, Kiviranta, & Helin, 2010), (Montonen, et al., 2012), (Yousefi, Handroos, & Soleimani, 2010), (Sinha, Liang, Paredis, & Khosla, 2001), (Yousefi, Soleimani, & Handroos, 2009), (Bauer & Rosen, 1997), (Kuusisto, Kaapu, Ellman, & Tiainen, 2012). Finding problems in the design, before building prototypes and expensive test setups, may lead to cost savings. The level of immersion of such simulation systems affects significantly its usefulness as a design tool (Kuusisto, Ellman, Kaapu, & Tiainen, 2011).

In (Korkealaakso, Rouvinen, Moisio, & Peusaari, 2007), (Xiaochen, 2011), (Kallmann, et al., 2003), (Peternier, Cardin, Vexo, & Thalmann, 2007) and (Heikkinen, 2009) construction of such R&D environments and its components had been discussed in details. An example of a VRERS is shown in Figures 1a and b.

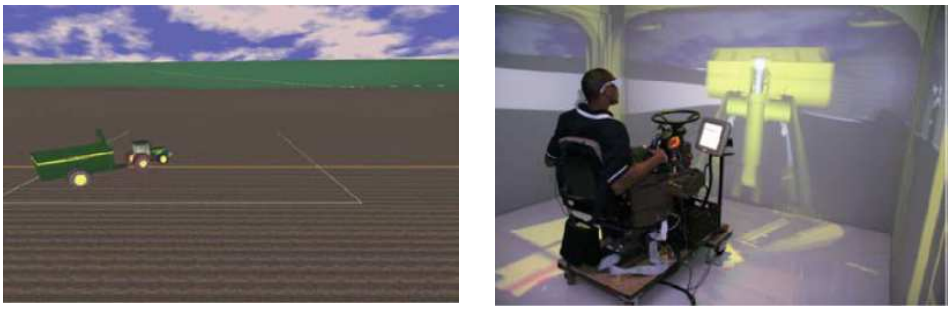

a) b)

Figure 1. a) A virtual farm scene with a tractor, b) Operator in the loop interface for real-time simulation with a four-sided CAVE Automatic Virtual Environment visualization (Karkee, Steward, Kelkar, & Kemp II, 2011).

In (Karkee, Steward, Kelkar, & Kemp II, 2011) a system for modelling and real-time simulation for virtual prototyping of off-road vehicles was developed. This architecture,

like many other similar systems, provides an environment to test functionality of controller software and hardware of virtual prototypes of mobile machines in real-time. Commercial software and components for VRERS are already available for instance, from (MeVea Ltd., 2013) and (Dassault Systemes, 2013).

Hardware-in-the-loop (HIL) setups are widely used in research and virtual prototyping; and are effective platforms for developing and testing real-time systems (Trigui, Jeanneret, Malaquin, & Plasse, 2007), (Timmermans, Van Mierlo, Lataire, Van Mulders, & McCaffree, 2007). For instance, in (Ahlawat, Jiang, Medonza, & Smith, 2012) transmission driven by an input dynamometer emulating the engine and output dynamometer emulating a vehicle was studied. According to the authors, this arrangement allows fast and accurate testing under realistic in-vehicle conditions and easy repeatability of tests. By using a HIL-setup, it is also possible to examine the dynamic phenomena inside hydraulic systems. In order to simulate hydraulic load, normally hydraulic components are used (Driscoll, 2005), (Guerrier & Edge, 2001), (Kővári, 2010), (Jiao, Gao, Hua, & Wang, 2004) (Enes & Book, 2008). In (Driscoll, 2005) hydraulic circuit shown in Figure 2 was designed to implement an emulation of a single-rod cylinder with two pumps. The pumps are actuated by electric motors and controlled by a real-time simulator.

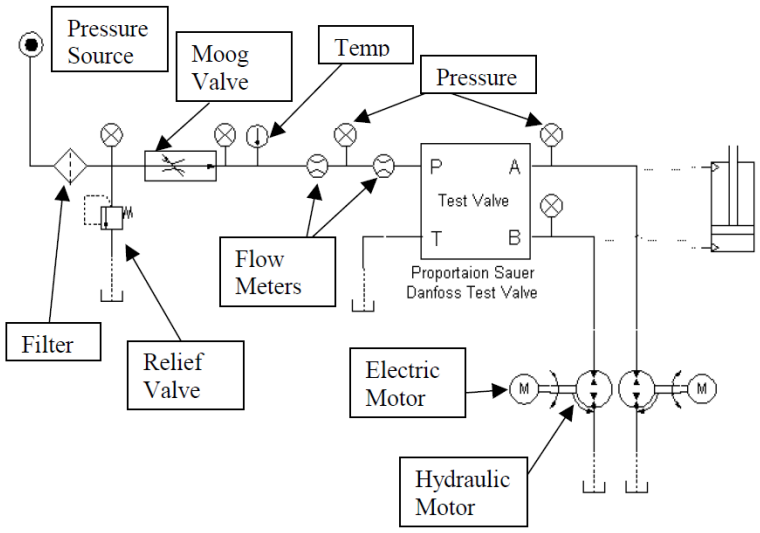

Figure 2. Hydraulic circuit diagram of a HIL simulation system for emulating a single-rod cylinder. Electric motors are controlled from a real-time simulator to simulate a single-rod cylinder as shown with dotted lines (Driscoll, 2005).

In (Kővári, 2010) trials were used to test the dynamic behaviour of the complete electro-hydraulic servo system. However, there is a lack of research on emulating

hydraulic systems themselves without hydraulic components. Therefore, the project of emulating a hydraulic pump by using an electric motor was initiated.

As humans rely on their senses to perceive their surroundings, the same senses are also needed to give information of the machines being driven (Gibson & Crooks, 1938). In addition to, for example, hearing if something is broken or what is the speed of the machine's motor, these things can also be felt with haptic senses as forces, vibrations, heat, joint orientations and even pain (Gibson & Crooks, 1938), (Enigk, Foehl, & Wagner, 2008). When using a virtual reality environment (VRE), a simulator and remotely operating a machine, some of the sensory cues are missing. Visual and audio sensory information is always taken into consideration, but forces, vibrations, heat and smells are often left out due to difficulties in providing them to the user. When sensory cues are missing, the efficiency of the human operation can be expected to be low (Nitsch & Färber, 2012) (Wildenbeest, Abbink, Heemskerk, van der Helm, & Boessenkool, 2012). In (Nitsch & Färber, 2012) it was proven that the efficiency of a human operated machine is higher compared to a teleoperated machine without force feedback.

In a simulator or a teleoperation system, motions and forces that the machine imposes on the operators body can be recreated with a motion platform (Figure 3) (InMotion Simulation, 2013), (Shiong, Jalil, & Hussein, 2009).

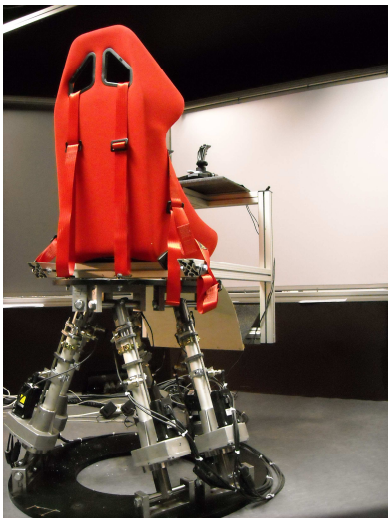

Figure 3. A motion platform with a rally seat and joysticks. (Heikkinen, 2009)

Vibrators can be used to mimic the vibrations of the machine which are outside the capability of the motion platform or just to give extra information of events.

In (Ryu, Chun, Park, Choi, & Han, 2010) the usability of vibrotactile messages in in-vehicle information communication was researched. Though further research was suggested in the article, the effectiveness and potential of communication with vibration was shown. While motion platforms and vibrators are commonly used in different applications, the manual controllers of mobile machines are mostly joysticks without force feedback. Gaming industry has however produced several commercial force feedback controllers. Other available haptic (force feedback) devices as (Geomagic, 2013), (Butterfly Haptics, 2013), (NovintFalcon, 2013) and (Force Dimension, 2013) are commercially available. Figure 4 presents three of the most common types of haptic devices.

a) b) c)

Figure 4. a) Phantom Premium, b) Magnetic levitation haptic device (Butterfly Haptics, 2013), c) haptic device by Force Dimension (Force Dimension, 2013).

Several studies have been made of the topic of novel haptic controllers and mobile machines (Takemoto, Yano, Miyoshi, & Terashima, 2004), (Hayn & Schwarzmann, 2009), (Kim, Won Oh, Hong, Park, & Hong, 2008) and (Parker, Salcudean, & Lawrence, 1993). In (Takemoto, Yano, Miyoshi, & Terashima, 2004) a joystick with added force feedback was presented for rotary crane teleoperation. It provided only two degrees of freedom (DOF) which is not enough for 6 DOF motions of a symbolic tool like presented in (Heikkinen, 2009). In (Hayn & Schwarzmann, 2009) a control concept for a hydraulic mobile machine was presented using Phantom Omni (Geomagic, 2013). This control concept is shown in Figure 5. According to the authors, it promises intuitive operation of the mobile working machine. Due to geometric similarities Phantom Omni haptic device is used to control an excavator. This requirement of geometric similarity restricts the use with other mobile working machines.

In (Kim, Won Oh, Hong, Park, & Hong, 2008) a haptic device is proposed and designed for the remote control of excavator style dismantling equipment used in dangerous working environments. In Figure 6, it can be seen that the device is just another modified joystick.

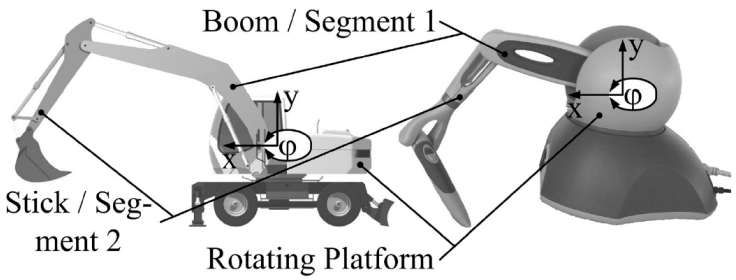

Figure 5. Analogy and geometry of a Phantom Omni device and an excavator boom (Hayn & Schwarzmann, 2009).

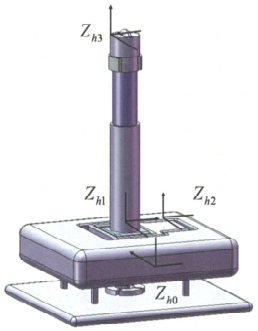

Figure 6. A haptic joystick for remote control of dismantling equipment. (Kim, Won Oh, Hong, Park, & Hong, 2008).

In (Parker, Salcudean, & Lawrence, 1993) a magnetically levitated joystick like in Figure 4b was used as a haptic device to control a hydraulic machine. A functional implementation for a Feller/Buncher shown in Figure 7 was suggested.

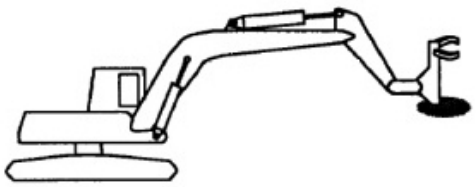

Figure 7. A typical Feller/Buncher (Parker, Salcudean, & Lawrence, 1993).

In (Villaverde, Raimúndez, & Barreiro, 2012) is presented a human machine interface for the operator of a gantry crane. It consists of a graphical interface showing a virtual model of a gantry crane to the operator (Figure 8c), haptic interface Phantom Omni (Geomagic, 2013) for force feedback (Figure 8b) and control of the crane (Figure 8a). User tests to verify the functionality of the system were made, but larger scale tests were recommend. It was concluded that the graphical interface needed enhancing. The setup and combination of the virtual device and the real one is impressive, but no attempt was made to consider the possibility of alternative choices for the haptic device used.

a) b) c)

Figure 8. a) Inteco 3DCrane, b) Phantom Omni, c) Graphical interface of the crane (Villaverde, Raimúndez, & Barreiro, 2012).

A VR user interface station shown in Figure 9a with hydraulics HIL-simulation for prototyping of excavator control systems was made in (Elton, Enes, & Book, 2009).

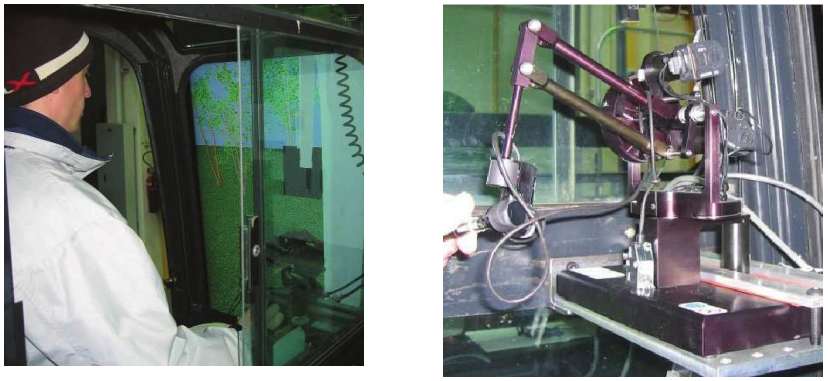

a) b)

Figure 9. a) An operator inside the operator interface station b) The haptic joystick for controlling a prototype excavator system (Elton, Enes, & Book, 2009).

A fully functional system was built for the testing of an excavator with a haptic device (Figure 9b), but authors settled for a generic commercial device instead of developing an alternative device for the application.

Figure 10 shows Phantom Premium 1.5 HF (Geomagic, 2013) used with a shovel for controlling a mine loader at LUT simulator laboratory. The natural motions of using a shovel were translated to mine loader actions.

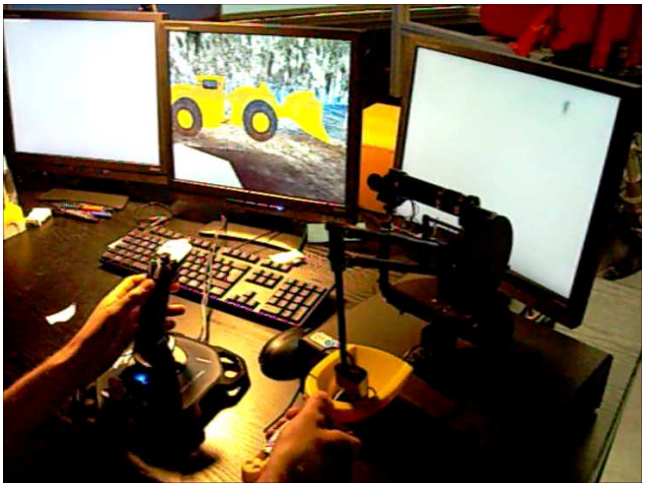

Figure 10. Phantom Premium, a shovel and a mine loader simulation.

After the tests with the shovel, the following conclusions were made. The box with electronics located as the bottom of the Phantom Premium was limiting the usable work area. Also it was unpractical to locate near driver's seat and always blocked the user's views. Due to these observations, a decision to find an alternative mechanical solution for a teleoperation haptic controller was made. For initial testing of the haptic controller a VRERS was designed and built.

1.2 Scope of the work

The first aims of the doctoral thesis are to develop an alternative mechanism for a haptic controller for mobile machine teleoperation and to test it with a VRERS. Second aim is the testing of simulator software with a HIL-setup to emulate a hydraulic pump with electric motor.

1.3 Scientific contributions

The main contributions of the work are the following.

1) An alternative configuration of mechanical structure for haptic controller was suggested for application of mobile machine control.
2) Analysis of electrical motors to emulate a hydraulic pump in HIL-simulators for electro-hydraulic hybrid transmissions system.

1.4 Author's contribution

All the innovations and ideas in these projects related to haptic controller and VRERS were made by the author under supervision of professor Heikki Handroos. The author was responsible for the design and realization of the VRERS at LUT. The test setup and prototype for the haptic controller testing was designed, programmed and mainly built by the author. All software made during the haptic controller and VRERS project which is not otherwise mentioned to be made by someone else was made by the author. User tests with the haptic controller were designed, arranged and conducted by the author. The experimental setup for the real-time HIL-simulation for testing of electric motor drives emulating a hydraulic pump was built on existing setup at LUT electric drives laboratory. The used control programs and the actual tests were made by the author and D.Sc. Tatiana Minav.

1.5 Outline of the Thesis

The following section presents the work carried out in this study.

In **Chapter 2,** a virtual reality environment with a simulator for research, design and testing of human machine interface is presented. Hardware and software of the system are described.

In **Chapter 3**, a HIL-simulator for testing of hydraulic machines with electric transmission hardware is described with an example setup and test results are shown. Analysis of using and choosing an electric machine to emulate a hydraulic pump in a HIL setup is presented.

In **Chapter 4,** an alternative mechanical structure for a haptic controller for mobile working machine is presented. Descriptions of its architecture, hardware, software and user tests are also given.

Chapter 5 provides the conclusions and recommendations for future research.

2 VRE with real-time simulator

Developments in VR technologies and real-time simulators (Heikkinen, Luostarinen, & Handroos, 2012) (Heikkinen, Minav, Handroos, & Pyrhönen, 2012) (Korkealaakso, Rouvinen, Moisio, & Peusaari, 2007) have enabled engineers to use them as R&D tools in mobile working machine applications. Therefore, the initial target of the research project at LUT was, to design and construct a VRERS. Following sections introduce the hardware, software and short recommendations for building a VRERS.

2.1 Hardware and software

Figure 11 shows a VRERS with a rubber tyred gantry (RTG) model at the LUT simulator laboratory.

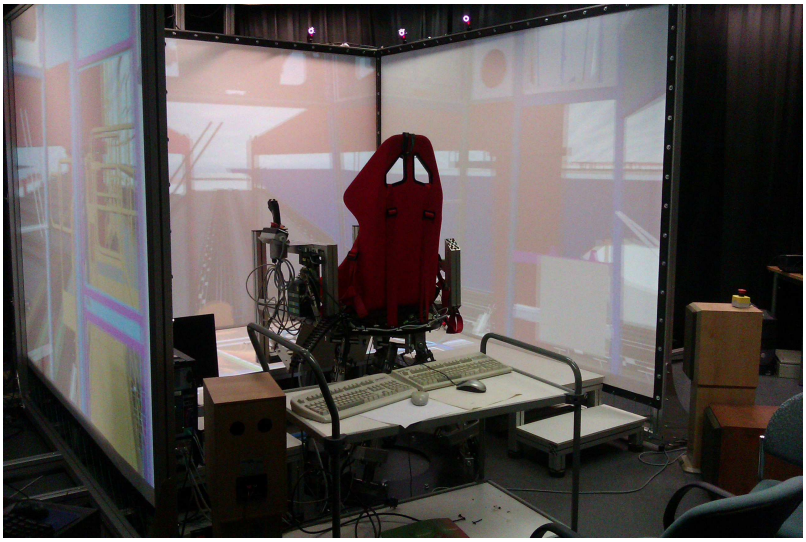

Figure 11. VRERS with a RTG model (Heikkinen & Handroos, 2013 b).

The four screens (in Figure 11) of the VRERS are in the front, on the sides and on the floor in front of the driver. The screens are attached to aluminium profile structures. The raised floor allows ease of climbing to the motion platform and underneath placement of cables. Projection surface of the floor was made from white coated chipboard.

The following hardware was used in the VRERS at LUT:

- Four Viewsonic's PJD6381 3D projectors (Viewsonic, 2013)
- Four NVidia 3D Vision Pro glasses and a transmitter (NVIDIA Corporation, 2013)
- Three 2.67 x 2.10 m sized Da-Lite Ultra Wide Angle rear projection screens (Da-Lite, 2013)
- 12 OptiTrack FLEX:V100R2 motion tracking cameras, two Optihubs and Tracking Tools software (Naturalpoint, Inc, 2013)
- 6 DOF Gough-Stewart type motion platform with Omron SGDH-04AW-0Y Servopacks and 6 UBA2RNI linear actuators by Servomech
- dSPACE real-time computer with ds1005 processor board
- Dell Precision T7500 with two Intel Xeon X5560 CPUs, a soundcard by Creative Technology Ltd. and two NVidia Quadro FX5800 GPUs connected together with SLI bridge.
- Dolby 5.1 Surround sound amplifier + speakers and a subwoofer
- A vibration generator by The Guitammer Company (The Guitammer Company, 2013)

Figure 12 shows the structure of the VRERS. Computer 1 is used for the graphics and audio of the VRE and for the real-time simulation. It is connected to four 3D projectors, 3D glasses' transmitter and to a Dolby 5.1 surround sound amplifier with five speakers and a subwoofer. A vibration generator is connected to the amplifier and placed under the driver's seat for higher frequency vibration reproduction. Computer 2 contains a motion tracking software and connects to 12 cameras with hubs. The motion tracking system is used for creating a changing perspective, according to user's head position and orientation. Naturalpoint Inc. recommended the use of 12 cameras, based on the sizes of the projection screens used at LUT. There are six cameras on top and six below the screens. In Figure 13 is shown the used Tracking Tools (Naturalpoint, Inc, 2013) program with the locations of the cameras. The program is used for configuring and calibrating the cameras, tracking defined rigid objects and serving position and orientation information thru its Virtual-Reality Peripheral Network (VRPN) interface.

Computer 3 contains the motion platform's control and monitoring software made by the author. Computers 1 and 3 are used to connect joysticks and other devices to the system as shown in Figure 12. Computer 4 is a dSPACE real-time computer which

contains the motion platform's controller for the servo drives. 1Gbps Ethernet with one central network switch is used to connect components of the VRERS together. With Ethernet, VRPN (VRPN, 2013) and TCP/UDP socket protocols are used. Other connections between components include USB, Profibus, RS485, analogue signals and digital parallel and serial connections.

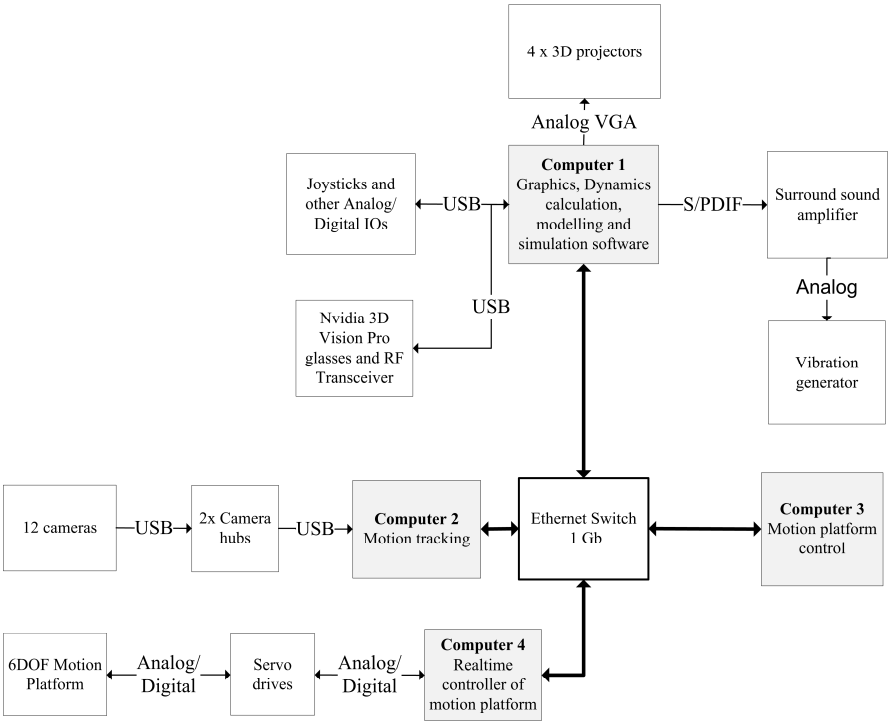

Figure 12. Structure of the VRERS.

Due to problems with functionality of Nvidia's 3D glasses' transmitter, USB connections are avoided on computer 1. A conflict between the transmitter and USB buses was solved by using mouse and keyboard with PS/2 connection instead.

During project, two different software packages were used to simulate mobile working machines. One of them is Virtools (Dassault Systemes, 2013) shown in Figure 14. This program was used for the graphics and the sound effects of a mobile machine. However, to calculate the real-time behaviour of the machine, additional customised program by MeVea (MeVea Ltd., 2013) was required.

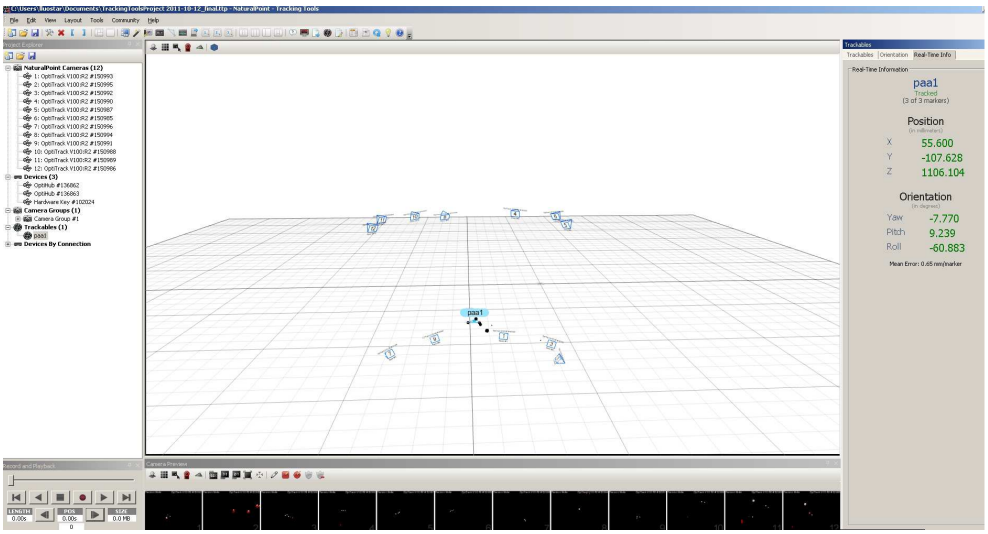

Figure 13. Tracking Tools (Naturalpoint, Inc, 2013).

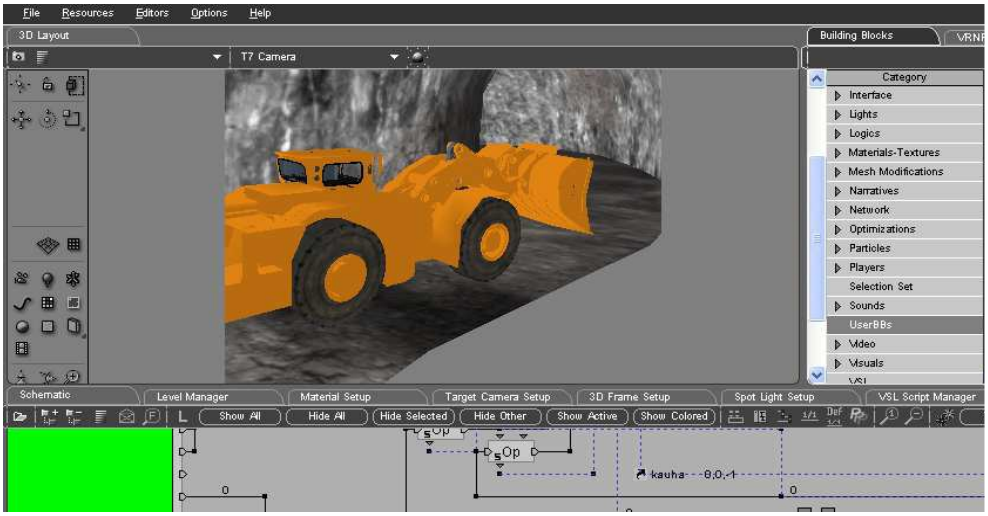

Figure 14. Virtools (Dassault Systemes, 2013).

Second package contains only software by MeVea. The MeVea modeller shown in Figure 15 is used for modelling the machine and its working environment. MeVea solver program calculates the machine model in real-time and creates audio and 3D graphics projected to the screens. This software allows using of external inputs and outputs to access variables inside the running real-time model. External connections can be made using Simulink blocks or a socket connection from users own program.

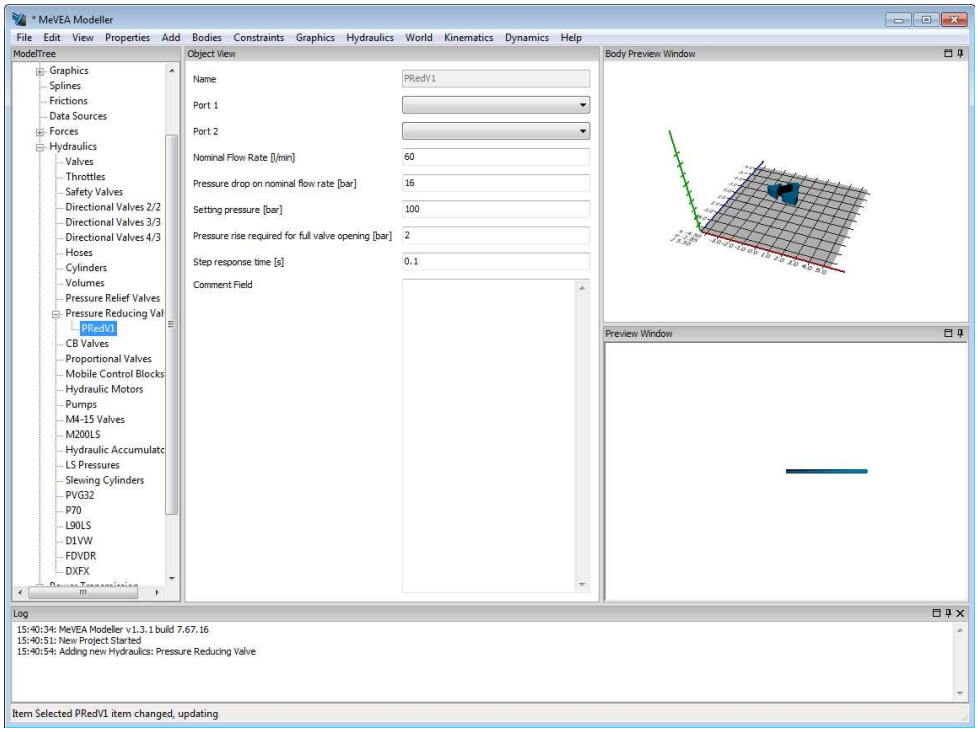

Figure 15. Modeller software (MeVea Ltd., 2013)

2.2 Recommendations for building a VRERS

This section contains recommendations based on the experience of designing and building the VRERS at LUT.

Consider the needed complexity, scale and detail of the machine and working environment models when choosing VRERS components.

Every computer should be optimised on the operating system level and any software or process that is not needed should be removed.

Separation of VRERS functions to different computers is recommended, to avoid interference between programs. Choosing the computer hardware for good parallel processing performance, allows easier application of multi-rate systems.

Latencies of data transfer and processing should be minimised. High data transfer rate can be useless with too much latency (Ramadoss & Hung, 2008). Artificial latency can be added later if needed for testing purposes.

Attention to used 3D graphics formats. Same format files from different CAD programs are not necessarily compatible.

3 Emulating a hydraulic pump with an electric machine in a HIL setup

This chapter is based on a project carried out with co-operation of Department of Electrical Engineering at LUT and results are published in (Heikkinen, Minav, Handroos, & Pyrhönen, 2012). To avoid the need to build or use a whole machine for testing, a hardware-in-the-loop (HIL) setup similar to those among others presented in (Leitner, 1996), (Petersheim & Brennan, 2008), (Sarikhani & Mohammed, 2012), (Lozoya-Santos, Tudon-Martinez, Morales-Menendez, & Ramirez-Mendoza, 2012) was used. Figure 16 shows a proposed HIL setup using a motor/generator for emulating the behaviour of a hydraulic pump. The setup contains a real-time simulator, two electric motors and two frequency converters. The real-time simulator is used for simulating the hydraulic and mechanical parts of a machine. The hydraulic pump emulator consists of an electric motor and a frequency converter. Its control signals are obtained from the real-time simulator. The emulator is seen as a load by the tested electric drive. Signal from the real-time simulator or a HMI is used to control the electric drive under test.

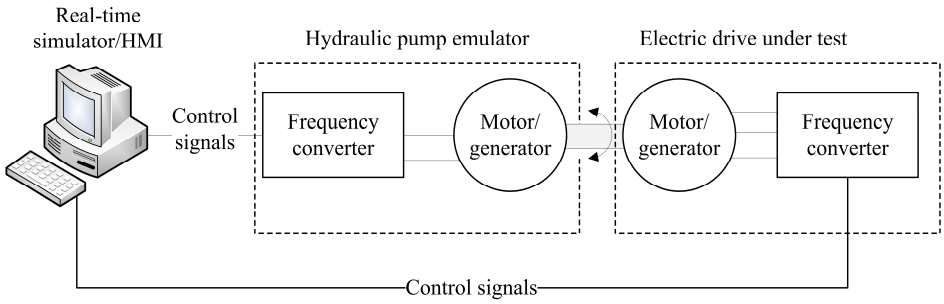

Figure 16. Proposed HIL setup using an electric motor for emulating the behaviour of a hydraulic pump.

Following sections introduce the hardware and software components of the realised HIL setup. The relationship between the simulated hydraulic pump and the emulator electric motor is discussed. Recommendations are given for choosing the electric motor for the emulating purposes of a hydraulic pump.

3.1 HIL setup hardware and software

A real-time model of a hydraulic boom based on a MeVea modeller tutorial was used and modified for this project. Figure 17 illustrates a picture of the boom. Reference data for comparison was obtained from measurements of a project (Minav, 2011) which used only the main lift function of a real electro-hydraulic forklift. Therefore, only the main cylinder of the boom was used by locking the other joints, in order to create similar

vertical motion as in the forklift. The used load was the arm of the boom with a weight of 384 kg.

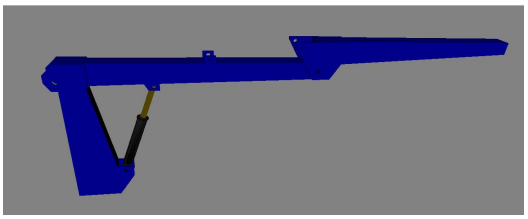

Figure 17. A picture of the simulated boom.

In Figures 18a and 18b are the simulated hydraulic circuits of the boom and the real main lift function of the forklift used for comparison. Both circuits have a single-acting cylinder, electric motor, hydraulic pump and a tank. In addition, the forklift has a two-way normally closed poppet valve and a pressure relief valve. The circuits are pump controlled systems without directional valves. During lowering motion, the pump acts as a hydraulic motor and rotates the electric motor as a generator.

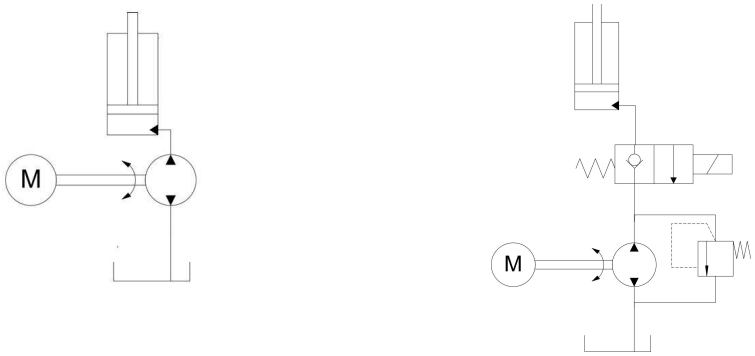

a) b)

Figure 18. a) Simulated hydraulic circuit of the boom, b) Hydraulic circuit of the main lift function of the forklift used for comparison.

The following differential equations were (Merritt, 1967) used for simulating the hydraulic components (Figure 18a) of the boom:

$$\dot{p} = \frac{B_e}{V_t}(Q_{pump} - Q_{cyl}), \tag{1}$$

$$Q_{pump} = D_p \omega_{act}, \tag{2}$$

$$Q_{\text{cyl}} = A_{\text{cyl}} \dot{x}_{\text{cyl}}, \tag{3}$$

$$T_{\text{pump}} = p \cdot D_{\text{p}}, \tag{4}$$

$$F_{\text{piston}} = p \cdot A_{\text{cyl}}, \tag{5}$$

where F_{piston} is the force of the cylinder piston, p is the hydraulic pressure and B_{e} is the bulk modulus of the system. V_{t} is the total volume of the hydraulic cylinder and tubes. Q_{pump} is the flow rate from the hydraulic pump and Q_{cyl} is the flow rate to the hydraulic cylinder. D_{p} is pump's displacement and ω_{act} is the actual speed of the emulator electric motor. A_{cyl} is the cross-sectional area of the hydraulic cylinder and $\dot{x}_{\text{cyl}}$ is the speed of the cylinder piston. T_{pump} is the torque on the pump shaft. Table 1 shows the parameters and values used in the hydraulic boom simulation.

Table 1. Values used in the hydraulic boom simulation.

Parameter	Value
Internal diameter of the cylinder, m	0.05
Length of piston rod, m	0.57
Diameter of cylinder piston rod, m	0.02
Internal diameter of pipe, m	0.02
Length of the pipe, m	0.03
Displacement of pump, m^3/rad	$3.02 \cdot 10^{-6}$
Bulk modulus of oil, MPa	1500
Effective bulk modulus of the system, MPa	1377

Figure 19 shows the hardware components and their connections in the realised HIL setup. Two ACSM1 frequency converters by ABB (ABB, 2013) were used in the setup: one with a brake resistor attached and the other one with its internal capacitor to storage the generated energy. Two ABB 1kW MS4813 motors were coupled together mechanically. Table 2 shows the motor parameters. The reference forklift system used a 10kW motor and the motors available for the HIL-setup were too small to lift the simulated boom. Therefore, the torque reference values for the emulator were divided by 10.

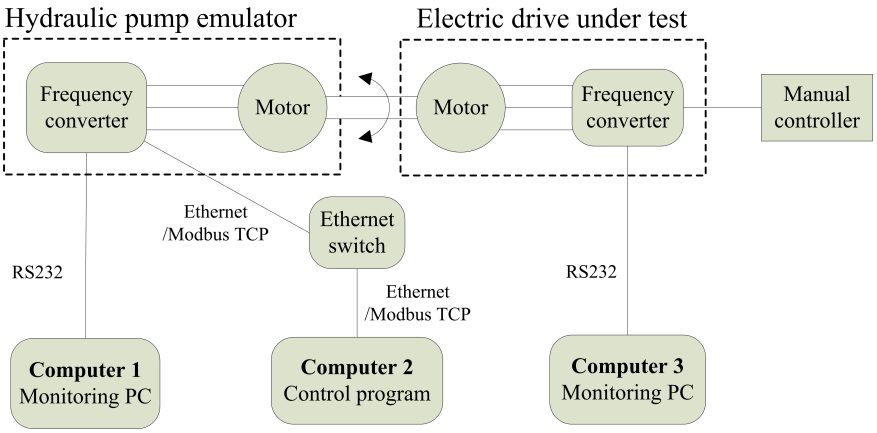

Figure 19. HIL test setup, components and connections.

Table 2. MS4813 motor parameters.

Parameter	Value
Rated torque, Nm	3.3
Maximum torque, Nm	9.9
Rated speed, rpm	3000
Maximum speed, rpm	4500
Voltage constant, V	202.3
Torque constant, Nm/A	1.11
Inertia, kgm^2	$2.59 \cdot 10^{-4}$
Power, kW	1
Rated current, A	3.4
Maximum current, A	9.3
Mechanical time constant, ms	1.7
Electrical time constant, ms	3.8

In Figures 19 and 20 are shown three computers used in the test setup. Computers 1 and 3 were used for monitoring and measuring data from the frequency converters via RS232 connections. Computer 2 contained control and real-time simulation software. It was connected to the emulator frequency converter using socket and Modbus/TCP connections via a 1Gbps Ethernet switch. Manual controller was used to control the tested motor and boom.

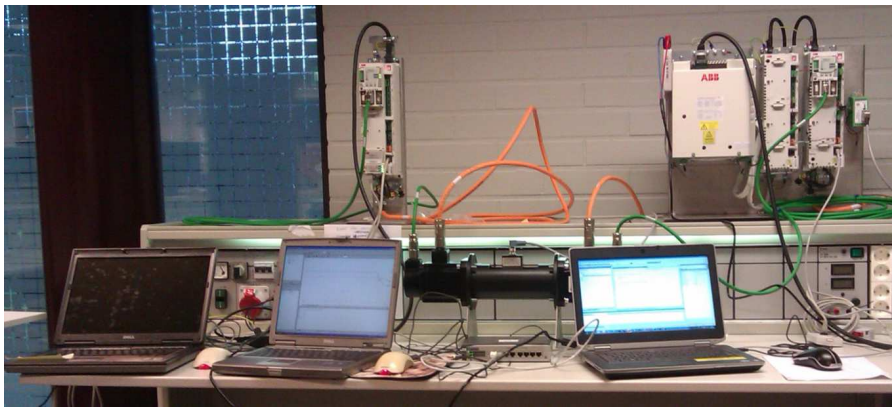

Figure 20. HIL setup in laboratory (Heikkinen, Minav, Handroos, & Pyrhönen, 2012).

In Figure 21 is shown the dataflow in the HIL setup. The control program in computer 2 read the actual speed of the emulator motor and sent back to frequency converter the reference torque value. It wrote cylinder force to and read the resulting cylinder position and speeds from the real-time simulator by MeVea. The emulator motor was driven with torque control and the tested motor with speed control. Computers 1 and 3 recorded the speeds and torques of both motors from the frequency converters with ABB Drivestudio software. A control program was made to connect the real-time simulator and the frequency converter together. The used version of the real-time simulator software did not have external access to all the needed variables of hydraulic components. Therefore, the simulation of the hydraulic components was included into the control program. The simulator program by MeVea simulated the mechanics of the hydraulic boom and the forces in the model. Figure 22 shows the functionality of the control program in the HIL setup. The program was divided into three parallel running threads. In this case, threads are parallel executed branches of a single program and do not define the distribution of execution between hardware components. Thread 1 was responsible for the graphical user interface: buttons, messages, errors and other information. Thread 2 handled the connection to the real-time simulator program using a socket connection. Cylinder position and force information was transferred between threads 2 and 3. Thread 3 calculated the torque for the emulator frequency converter, the cylinder force for the boom and the flow rate for the hydraulics. It read the acting speed and position from the emulator frequency converter. Thread 3 also saved all the used

data to hard drive for later analysis. Synchronisation of the threads was realised with semaphores and critical code sections locking the use of variables used for data exchange between threads. Problems with synchronisation were not observed. Modbus/TCP connection between the control program and the ACSM1 frequency converter was made with Free Windows Modbus Master library (Saat, 2012). Control program was made with Microsoft Visual Studio (Microsoft, 2012) using MFC libraries.

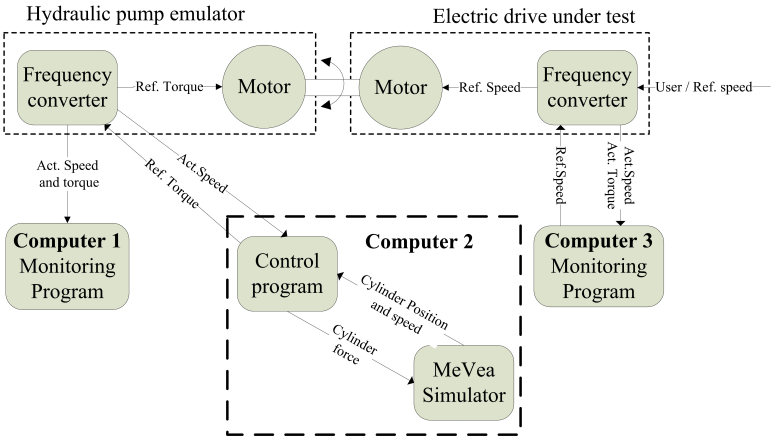

Figure 21. HIL control program flowchart (Heikkinen, Minav, Handroos, & Pyrhönen, 2012).

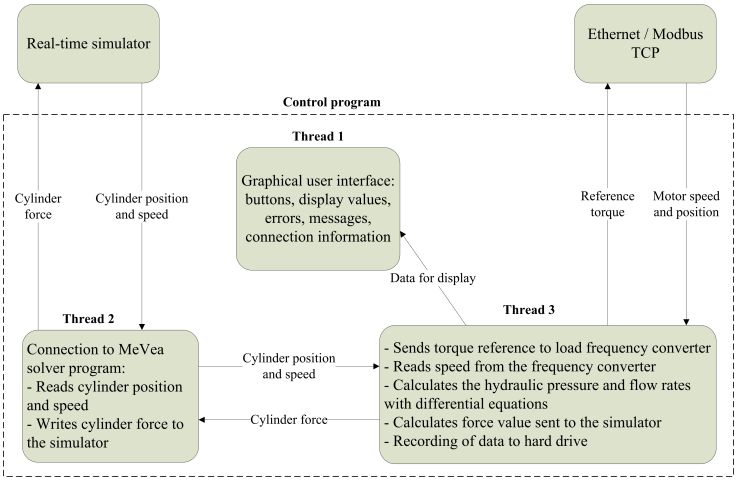

Figure 22. Functionality chart of the control program.

3.2 **Analysis of measurement results**

Figure 23 shows the measured speed and torque of the electric motor from the electro-hydraulic forklift setup (Minav, 2011). Motor torque is estimated by an ACSM1 frequency converter. Starting from 5 to 25 seconds, load is being lifted to maximum height. After 25 seconds, movement was stopped for 1 second and the direction of motion was changed. From 26 to 46 seconds, the load was going downwards until stopped and kept still.

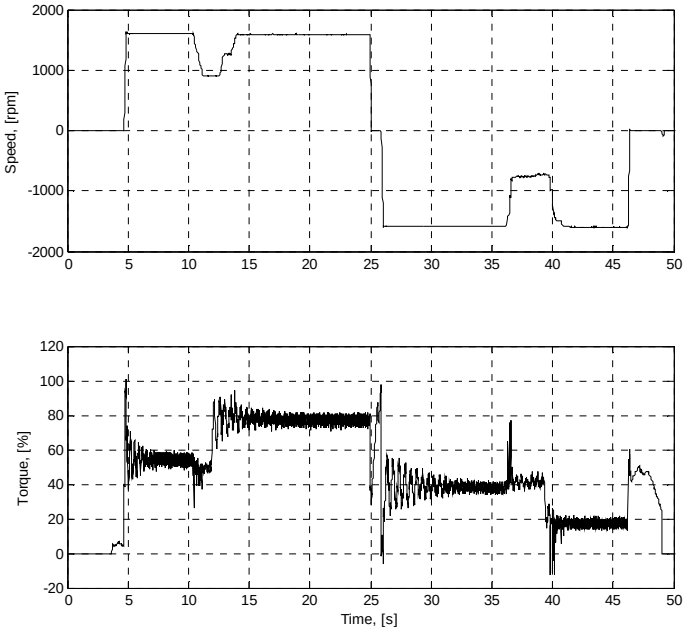

Figure 23. Measured data from the forklift setup: motor speed and torque.

Figures 23 and 24 are of the same event, the time scales are different due to separate data sources. Figure 24 shows the measured data for a forklift lifting/lowering cycle: system pressure, height of the forks from the ground and the velocity of the forks. Starting from 0 to 20 seconds, the load was being lifted to a height of 4.3 meters. After 20 seconds, forks were stopped for 1 second and the direction was changed. From 21 to 42 seconds, the forks were moving down with 0.3 m/s velocity until stopped and kept still. The recorded torque and pressure change in magnitude during motions due to changing structural payload of the forklift.

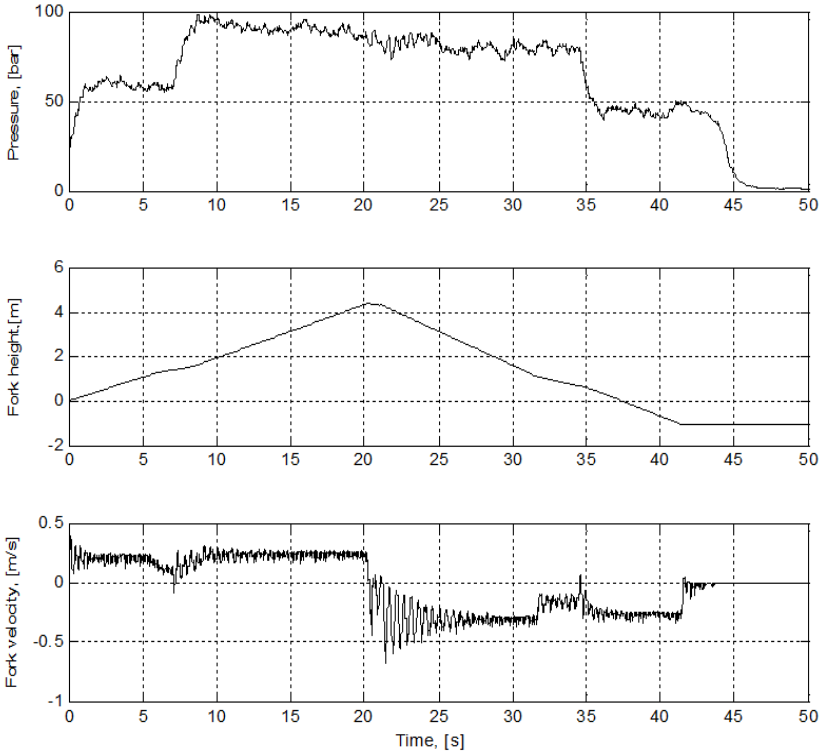

Figure 24. Measured data from the forklift setup: pressure, fork height and velocity.

In Figure 25 is the recorded data from the frequency converters of the emulator HIL-setup. Red line represents the motor to be tested and black line is the emulator motor. Both sides of the system behaved as expected and the event recordings were synchronous to each other.

Starting from 3 seconds to 14, the hydraulic cylinder was lifting the boom up from the ground. From 14 to 18 seconds, the boom arm was kept still by the test motor while the emulator motor was exerting a continuous load to it. At 18 seconds, the boom arm was going down until stopped at 26 seconds and kept still for 2 seconds until simulation was stopped. When simulation was stopped the torque was set to zero and the data is not usable after that point.

The boom upwards direction happened to be negative for the tested motor. As the motors are attached opposite each other from their axes, the directions of the emulator motor are inversed. For emulator motor, up direction would be positive direction of rotation. The emulator is trying to resist the upwards motion and it causes direction of the torque to be negative in value. During lowering, the emulator torque direction does not change as it is caused by the gravity on the boom arm. However, the tested motor is

trying to slow down the lowering motion and still applying negative torque. Therefore, the torque curves in Figure 25 are negative during lifting and lowering of the boom.

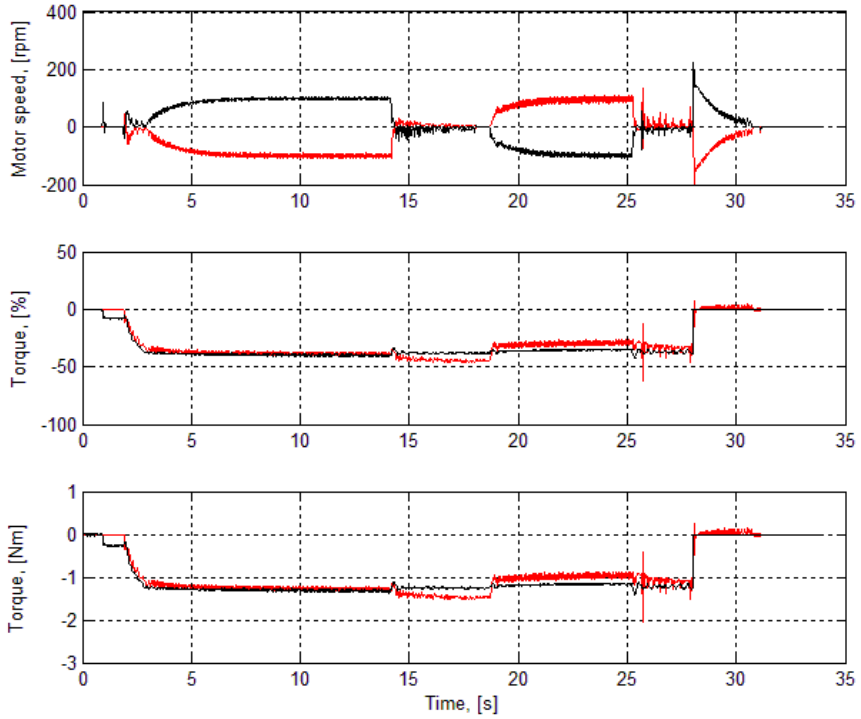

Figure 25. Recorded data from the emulator HIL-setup, red line is the tested motor and black line is the emulator motor (Heikkinen, Minav, Handroos, & Pyrhönen, 2012).

Figure 26 shows the recorded data from the control program and the real-time simulator software: cylinder piston velocity, system pressure, cylinder piston position and the flow rate from the pump. The pressure in the system rose in the beginning up to approximately 4.2 MPa until the force was big enough to lift the boom up. At 14 seconds, the boom was stopped and kept still until 18 seconds. After that the boom was lowered down and the velocity of the cylinder piston became negative. The pressure had a slightly lower value compared to the upwards motion as it was in the forklift measurements in Figure 24. The flow rate from the pump followed the behaviour of the motor speed.

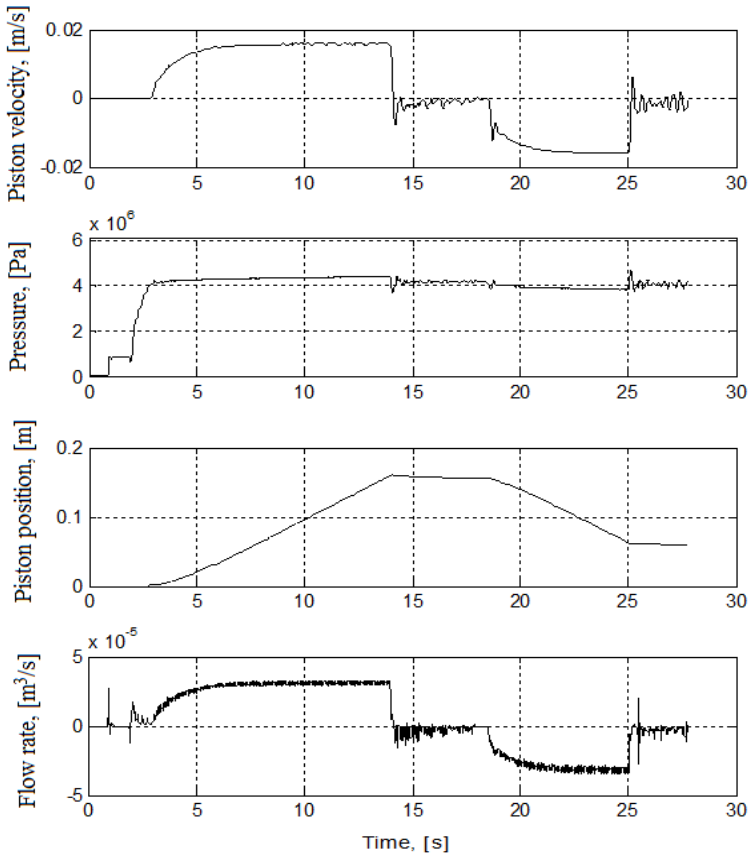

Figure 26. Recorded data from the control program and real-time simulator of the emulator HIL-setup: cylinder piston velocity, system pressure, the cylinder piston position and the pump flow rate. (Heikkinen, Minav, Handroos, & Pyrhönen, 2012)

Figure 25 and 26 were compared to the reference data (Figure 23, 24) from the hydraulic forklift setup (Minav, 2011). The recorded data from both tests showed the same behaviour in up, hold in place and lower down motions.

Figure 27 illustrates the cylinder piston velocity (red line) in m/s obtained from the real-time simulator. For clarity, the amplitude of velocity was scaled up by 100 to fit into the figure with torque. In the same figure is placed the torque curves of both test (black line) and emulator (blue line) motors in percents. Values are obtained from their frequency converters. The timings of the events shown by the curves appear to match each other. At the refresh rate of 1 kHz of the real-time simulator, the cylinder piston velocity curve looks smooth in the enlarged portion. The changes in oscillations match each other in all the curves. However, the torque curve of the tested motor has more

oscillations than the emulator motor. This is a result of the tested motor being controlled with speed and the emulator motor with torque. The measurement frequency of the torque values was 100 Hz and was obtained from the smallest recorded time interval of the data.

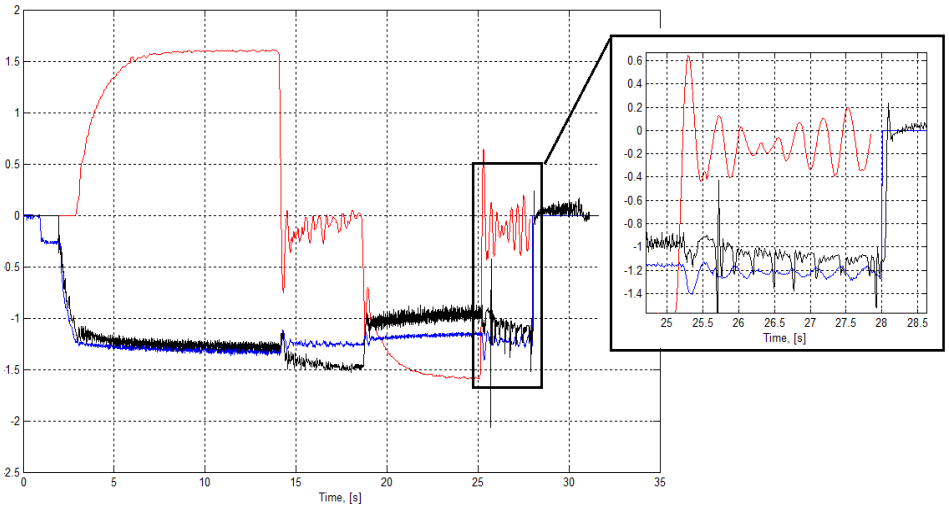

Figure 27. Cylinder piston velocity from real-time simulator (red line), black line is the torque of the tested motor and blue line is the torque of the emulator motor.

3.3 Requirements for the HIL setup to emulate a hydraulic pump

There are two initial criteria for choosing an electric motor to be an emulator of a hydraulic pump in a HIL-setup. A first criterion is the refresh rate of the electric motor. The second criterion is the pressure/flowrate curve of the emulator electric motor in relation to pump specifications of the simulated hydraulic circuit.

3.3.1 Refresh rates of the HIL components

Refresh rates of each component were obtained from datasheets, measurements, by calculation or by estimation. To calculate the torque control refresh rates of the electric motors the following transfer functions were used. The open-loop transfer function for a simplified torque controlled permanent magnet servomotor can be derived from DC-motor transfer functions (Franklin, J, & Emami-Naeini, 1986). The equations of equivalent electrical circuit for a DC-motor are:

$$L_{\text{coil}}\dot{I} + R_{\text{a}} I = U - K_{\text{e}}\omega_{\text{shaft}}, \tag{6}$$

$$T_{\text{em}} = K_{\text{m}} I, \tag{7}$$

where K_{e} is voltage constant, L_{coil} is coil inductance, R_{a} is coil resistance, U is supply voltage, I is current, T_{em} is torque of the electric motor, K_{m} is torque constant and ω_{shaft} is the angular speed of the shaft. The equation of motion with a simple inertia moment of rotor J_{mrotor} load becomes

$$J_{\text{mrotor}}\dot{\omega}_{\text{shaft}} + b_{\text{m}}\omega_{\text{shaft}} = T_{\text{em}} = K_{\text{m}} I, \tag{8}$$

where b_{m} is viscous friction coefficient.

By assuming low speed, the back electromotive force (EMF) voltage $K_{\text{e}}\omega_{\text{shaft}}$ in (6) can be neglected; the transfer function between motor voltage U and angular speed ω_{shaft} from (6) to (8) can be obtained as follows:

$$W(s) = \frac{\omega_{\text{shaft}}(s)}{U(s)} = \frac{K_{\text{m}}}{R_{\text{a}} b_{\text{m}} \cdot (\tau_{\text{f}} s + 1) \cdot (\tau_{\text{m}} s + 1)}, \tag{9}$$

where τ_{f} is electrical time constant and τ_{m} is mechanical time constant:

$$\tau_{\text{f}} = \frac{L_{\text{coil}}}{R_{\text{a}}}, \tag{10}$$

$$\tau_{\text{m}} = \frac{J_{\text{mrotor}}}{b_{\text{m}}}. \tag{11}$$

Equations (10) and (11) are commonly used in describing time constants in electrical motors. However, in HIL-system instead of using speed control in the pump emulator motor, torque control is used. By assuming the motor shaft is flexible and it is rigidly mounted in a frame, Equation (8) can be updated as follows:

$$J_{\text{mrotor}}\ddot{\theta} + b_{\text{m}}\dot{\theta} + C\theta = T_{\text{em}} = K_{\text{m}} I, \tag{12}$$

where θ is the rotor angle. C is the spring constant of shaft (Airila, et al., 1995) and can be calculated as:

$$C = \frac{\pi \cdot {D_{\text{mshaft}}}^4 \cdot G}{32 \cdot L_{\text{mshaft}}}, \tag{13}$$

where G is shear modulus of steel, D_{mshaft} is diameter of motor shaft and L_{mshaft} is the length of the shaft. The transfer function can be derived from Equations (6), (7) and (12) as a ratio between voltage U and load torque $T_{\text{out}} = C \cdot \theta$ as follows

$$W(s) = \frac{T_{\text{out}}(s)}{U(s)} = \frac{K_{\text{m}}}{R_{\text{a}} \cdot (\tau_{\text{f}} s + 1) \cdot (\tau_{\text{m1}} s^2 + \tau_{\text{m2}} s + 1)}, \tag{14}$$

where

$$\tau_{\text{f}} = \frac{L_{\text{coil}}}{R_{\text{a}}}, \tag{15}$$

$$\tau_{\text{m1}} = \frac{J_{\text{mrotor}}}{C}, \tag{16}$$

$$\tau_{\text{m2}} = \frac{b_{\text{m}}}{C}, \tag{17}$$

where τ_{f} is electrical time constant, R_{a} is resistance, τ_{m1} and τ_{m2} are mechanical time constants, J_{mrotor} is inertia of the rotor, b_m is viscous friction coefficient, K_{m} is torque constant.

Since the shaft compliance is evident, with the final value theorem and from Equation (14) a simplified transfer function was obtained:

$$W(s) = \lim_{C \to \infty} \frac{K_{\text{m}}}{R_{\text{a}} \cdot (\tau_{\text{f}} s + 1) \cdot (\tau_{\text{m1}} s^2 + \tau_{\text{m2}} s + 1)} = \frac{K_{\text{m}}}{R_{\text{a}} \cdot (\tau_{\text{f}} s + 1)}. \tag{18}$$

Equation (18) shows that the mechanical time constant can be neglected in torque controlled pump emulator motor. Therefore, the dynamic properties of the motor are fully dominated by the electrical time constant.

Transfer function from Equation (18) was used for step response analysis of electric motor. The torque refresh rates were calculated with Equation (19) using the settling time of the step response analysis.

$$f_{\text{refresh}} = 1/T_{\text{settling}}, \tag{19}$$

where f_{refresh} is the maximum digital signal frequency, T_{settling} is settling time.

Three motors were analysed and compared and Table 3 shows their parameters. The motor MS4813 chosen initially for testing was too small with regards to torque and its reference values were divided by 10 in the simulator software. As a result, a sufficiently sized motor MS4889 from the same motor series was evaluated. A motor BLS-144 from Mavilor was chosen also for comparison.

Table 3. Motor parameters.

Parameter	ABB: MS4813	ABB: MS4889	Mavilor: BLS-144
Rated torque, Nm	3.3	35.8	33
Maximum torque, Nm	9.9	89.5	132
Rated speed, rpm	3000	2000	-
Maximum speed, rpm	4500	3000	6500
Torque constant, Nm/A	1.11	1.76	4.52
Inertia, x 10^{-4} kgm^2	2.59	57	0.459
Power, kW	1	7.5	-
Mech. time constant, ms	1.7	0.8	1.61
Elec. time constant, ms	3.8	14.2	4.4
Resistance, Ω	5.73	0.3	2.5
Shear modulus of steel, MPa	78500	78500	78500
Diameter of motor shaft, m	0.0215	0.03	0.024
Length of shaft, m	0.04	0.06	0.05

In Figure 28 is the step response of the motor MS4813. As it takes the motor 0.0149 seconds to reach its reference torque value, it can follow a digital signal with a refresh rate of 67 Hz. Appendix A contains bode plots and bandwidth data of the motors.

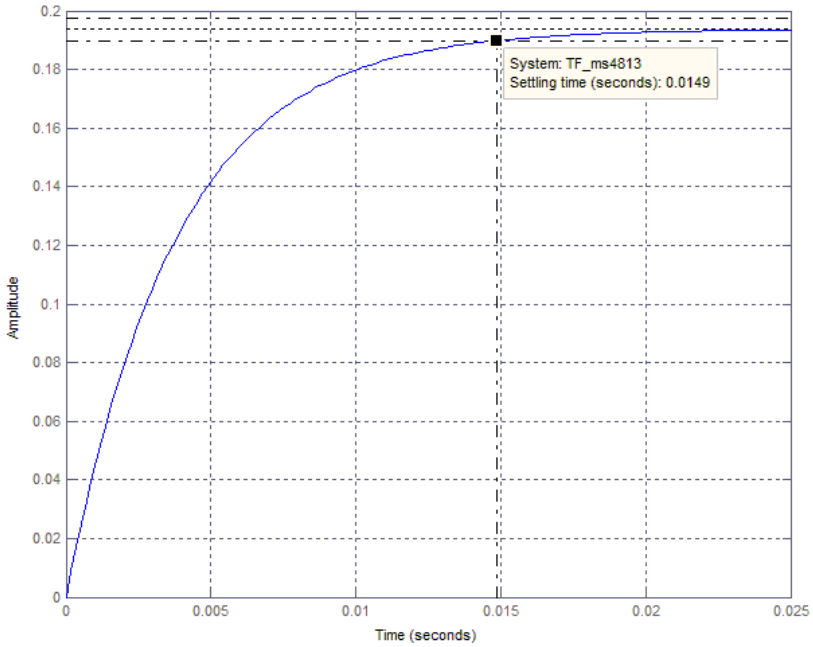

Figure 28. Step response and settling time of the MS4813 motor.

In Figure 29 is the step response of the MS4889 motor. It takes the motor 0.0556 seconds to reach its reference torque value and it can follow a reference signal with a refresh rate of 17 Hz.

In Figure 30 is the step response of the BLS-144 motor. The motor reaches its reference torque value in 0.0172 seconds and it can follow commands with a refresh rate of 58 Hz.

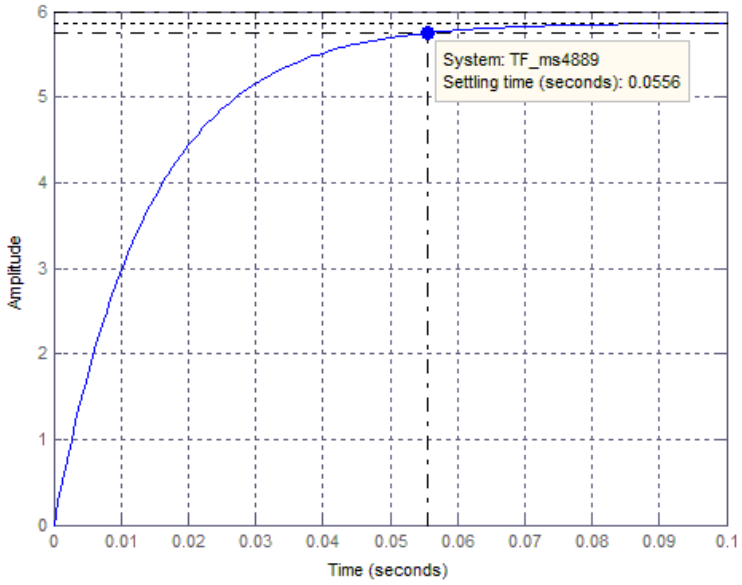

Figure 29. Step response and settling time of the MS4889 motor.

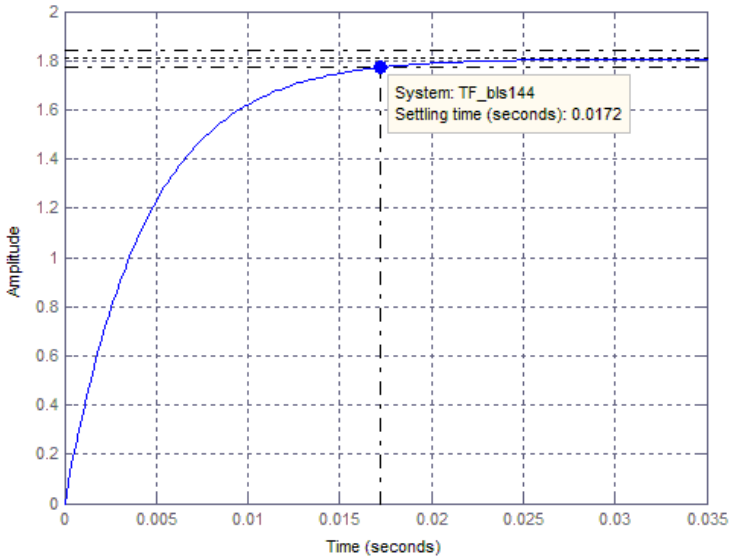

Figure 30. Step response and settling time of the BLS-144 motor.

Table 4 shows the refresh rates of used and suggested HIL-setup components.

Table 4. Refresh rates of HIL-setup components.

Component	Frequency [Hz]
Real-time simulator of boom	1000
Control program	333 - 1000
Modbus/TCP/frequency converter	100
Measurements from frequency converter	100
Simulator graphics	30
Human operator	5
MS4813 motor	67
MS4889 motor	17
BLS-144 motor	58

According to Table 4, as the source of all events in the setup, the real-time simulator has the highest refresh frequency of 1 kHz. This value refers to the maximum refresh rate for an external connection to the simulator. In ideal case this would be the target for all other components of the setup. The control program running in a Windows based PC could achieve the rate of 1 kHz, but mostly stayed closer to 333 Hz. Connection from the control program to the frequency converter was limited to an approximate 100 Hz. The ABB MS4813 motor used could do maximum 67 Hz based on the settling time analysis. The maximum action frequency of the human lifting and lowering the boom is around 5 Hz and the graphics of the boom was updated at 30Hz. Latencies were excluded from this analysis. Though the motor at 67 Hz was slower than other components of the setup, the 30 Hz rate of the graphics observed by the operator as a source of control information guaranteed sufficient functionality from the human point of view. The slow rate of the human actions also makes the motors 67 Hz sufficient in this setup. However, MS4889 motor could only reach 18 Hz. Its mechanical time constant was half of that of the MS4813 motor used, but the electrical time constant was almost four times bigger. BLS-144 has almost the same nominal torque and a higher maximum torque and speed as the MS4889, but has refresh rate of 58 Hz. This puts this motor close to the MS4813 used, but with better torque and speed characteristics.

3.3.2 Flowrate/Pressure evaluation of electric motor

Equations (20) and (21) are used to convert emulator electric motor's torque/speed curve into an emulated pump's pressure/flowrate curve.

$$\Delta p = \frac{T_{\text{pump}} \cdot \eta_{\text{HM}}}{\text{D}_\text{p}}, \tag{20}$$

where Δp is pressure difference across the pump, T_{pump} is torque, η_{HM} is hydro-mechanical pump efficiency, D_p is pump displacement.

$$Q_{\text{epump}} = \omega_{\text{epump}} \cdot D_\text{p} \cdot \eta_{\text{vol}}, \tag{21}$$

where Q_{epump} is flow rate of emulated pump, η_{vol} is volumetric pump efficiency, ω_{epump} is motor speed.

In the Figures 28, 29 and 30, the volumetric and hydro-mechanical efficiencies have been taken into account with some simplifications like, for example, excluding the effect of temperature change.

Figures 31, 32 and 33 show the emulator motor torque/speed curve converted into an emulated pump pressure/flowrate curve. The motors' curves are compared to the area of operation of a hydraulic internal gear pump EIPS2-13 with a displacement of the 13.3 cm^3/rev from Eckerle (Eckerle Industrie-Elektronik GmbH, 2013). This pump was used for testing with the forklift setup (Minav, 2011). In Figure 31 are shown both the real emulation capability of the MS4813 motor and the one reached by multiplication/division by 10 in the control program. The continuous pressure range can with multiplication barely reach 15 MPa, but the motor seems to be suitable for the boom setup due to its operational frequency.

Motor MS4889 in Figure 32 are more suitable for use in the boom setup as it can reach the multiplied MS4813 ratings with nominal torque. Due to the big electrical time constant and thus low frequency, it is suitable only for hydraulic circuits which do not require much from dynamic performance.

Figure 33 shows an electric motor chosen from Mavilor range of servomotors. Despite the similar nominal power and torque values with MS4889, it can provide a much higher frequency and momentary torque.

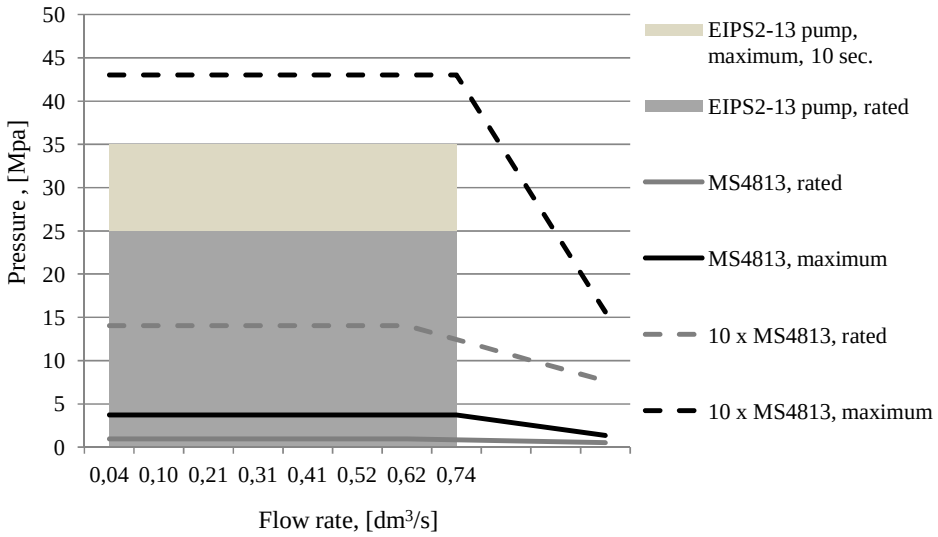

Figure 31. MS4813 pressure/flowrate curve.

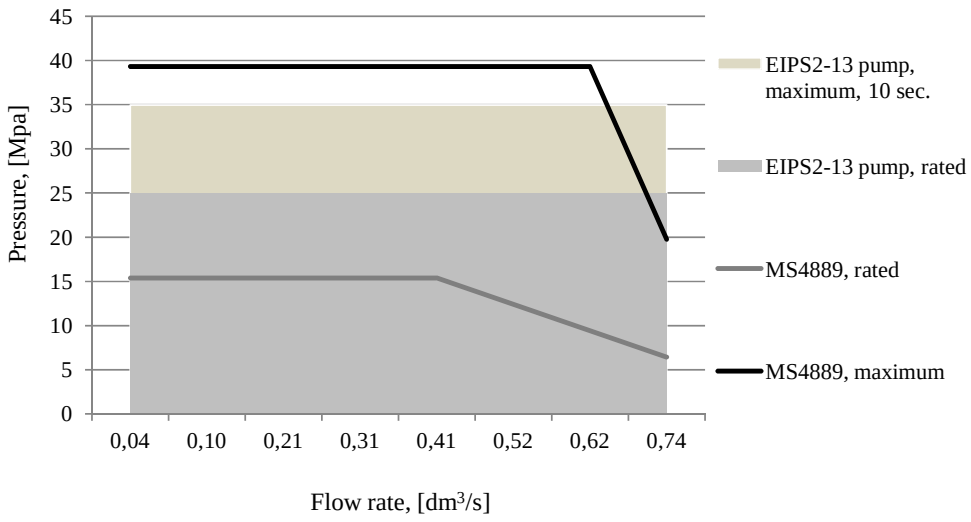

Figure 32. MS4889 pressure/flowrate curve.

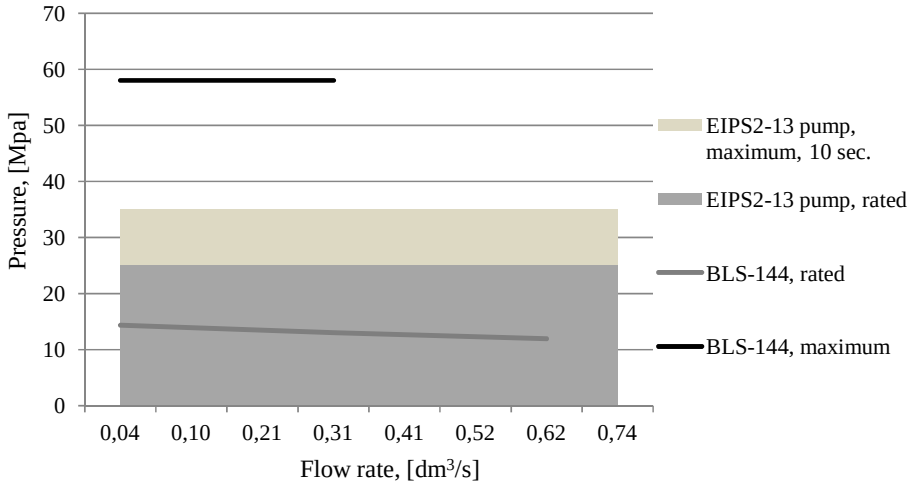

Figure 33. BLS144 pressure/flowrate curve.

3.4 Summary

In this research, it was shown that a virtual model of a hydraulic machine in a HIL setup can be used for testing by emulating the hydraulic pump with an electric motor. The components of this kind of test setup need to be chosen carefully: optimised for data transfer speed, low latency and suitable refresh rate. The electric motor for emulation of a hydraulic pump should be chosen based on the refresh rate and pressure/flowrate curves.

An electric motor designed for the purpose of emulating a hydraulic pump, should be considered in the future. Small electrical time constant and the torque characteristics of the motor are the main guidelines for this design.

4 Haptic controller for mobile machine teleoperation

In this chapter, a comparison is made between mechanisms of Phantom Premium 1.5 HF and two alternative haptic controllers. The VRERS from chapter 2 was used as a test environment for two prototypes. The test setup and prototype hardware and software are described. In the end of the chapter, user tests and analysis of results are presented.

Matlab 2013a, Symbolic toolbox and Robotics Toolbox Release 9 (Corke, 2013) were used for analysing the mechanisms in this chapter.

Mechanisms of the Phantom Premium and the two haptic controller prototypes were created into Matlab using Denavit-Hartenberg parameters in the Robotics Toolbox. Symbolic forward kinematics and Jacobian matrixes were created with Robotic and Symbolic toolboxes. The presences of kinematic singularities of the mechanisms were evaluated with the rank of their Jacobian matrixes as defined in (Donelan, 2010):

"A serial manipulator with kinematic mapping $f: Q \to G$, where the joint space Q has dimension k and the displacement group G has dimension n, has a **kinematic singularity** at $q \in Q$ if rank $T_q f$ has rank less than both k and n.", where $T_q f$ is a linear transformation, whose matrix representation is simply the Jacobian matrix $J\ f\ (q)$. The forward kinematics was used for calculating the workspace of the mechanisms and presents them as 3D point clouds. In Appendix B is shown the commands for making the singularity analyses with Matlab and Robotics Toolbox.

4.1 Phantom Premium 1.5 HF

Phantom Premium 1.5 HF in Figure 34 is a haptic interface device by Geomagic. The device has 6 DOF and force feedback in 3 DOF.

In Table 5, the Modified Denavit-Hartenberg parameters of the Phantom Premium 1.5 are shown.

Table 5. Modified Denavit-Hartenberg parameters of the Phantom Premium 1.5 (Hu, 2009).

i	α_{i-1}	a_{i-1}	d_i	θ_i
0	-π/2	0	0	- π/2
1	0	0	0.17 m	θ_1
2	π/2	*0*	0	θ_2
3	0	0.215 m	0	- π/2-θ_2+θ_3
Tool	- π/2	0.17 m	0	π/2

Where $\theta_{1,2,3}$ are angles of joints, d_i , a_{i-1}, α_{i-1} are Modified Denavit-Hartenberg parameters.

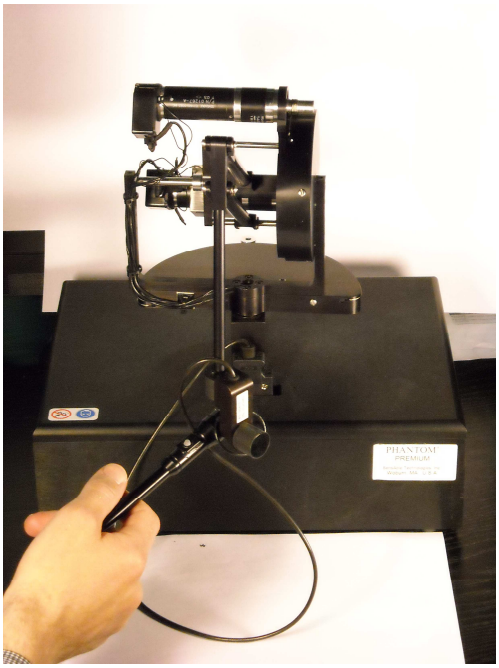

Figure 34. Phantom Premium by Geomagic.

In Figure 35 is shown the workspace of the Phantom Premium 1.5 HF with a view from the top. According to the analysis (Appendix B) there were no kinematic singularities inside the workspace. Only singularities are in the extremities of the workspace.

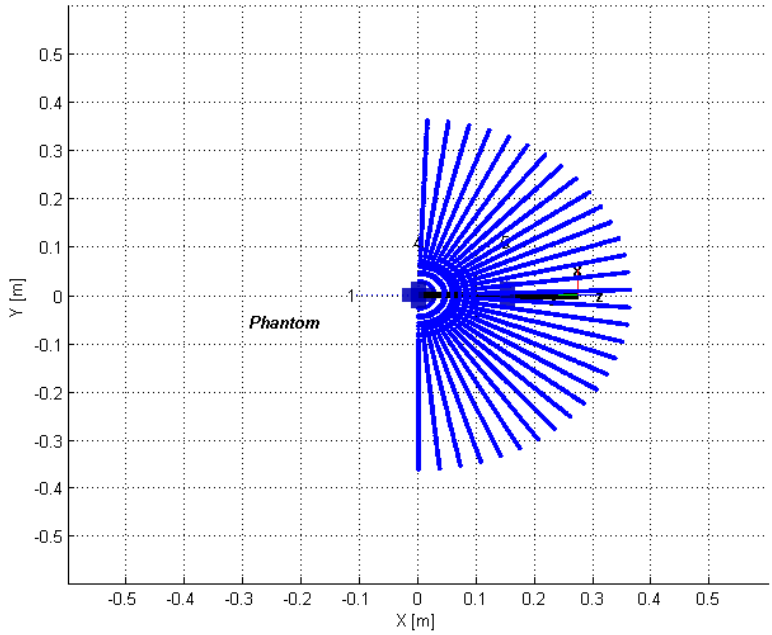

Figure 35. View of the workspace of Phantom Premium 1.5 HF from the top

In Figure 36 is shown the Phantom Premium's work space sliced from the side with the electronics box also shown in Figure 34. The box with electronics located as the bottom of the Phantom Premium limits the usable work area. Also the device was unpractical to locate near driver's seat and the mechanism often blocked the user's views. Control motions that were usable in the middle of the workspace became impossible in the extremities. This was due to limited workspace and losing of degrees of freedom. Therefore, user was limited to starting control motions only from the middle of the workspace.

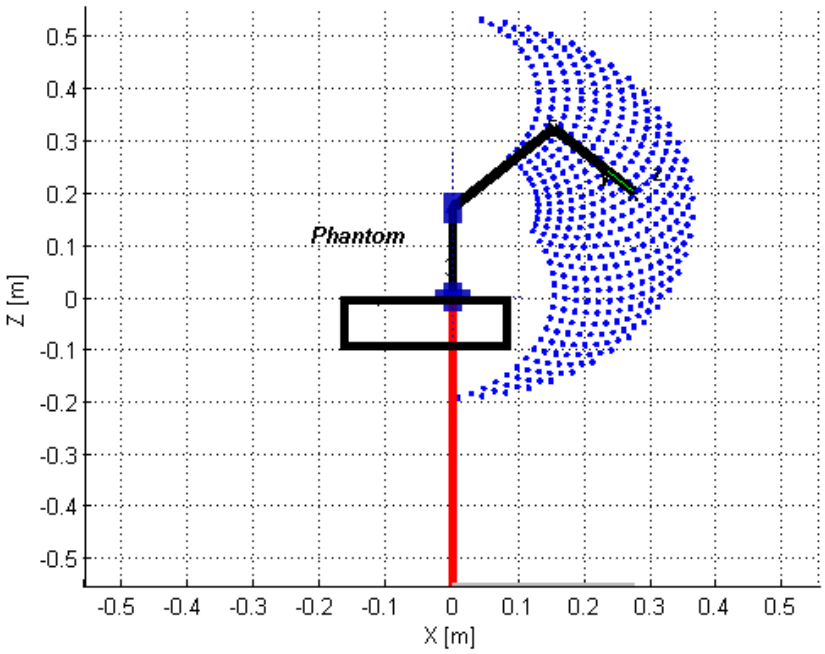

Figure 36. Workspace of Phantom Premium 1.5 from the side with square which represents the electronics box, joint rotating around Z axis is locked for the image.

Figure 37 shows a 3D view of the same workspace as in Figure 36. In Figure 38 is shown the gimbal and stylus of the Phantom Premium haptic device. A small children shovel was attached to the gimbal in (Heikkinen, 2009). Other similar symbolic handles like a box resembling a container were decided to try also, but the gimbal was too small in size.

Due to reasons mentioned in section 4.1, a decision to find an alternative mechanical solution was made. Following are the initial requirements for the mechanical structure:

- Bigger gimbal than in Phantom Premium,
- Larger usable workspace,
- No big electronics box underneath the device.

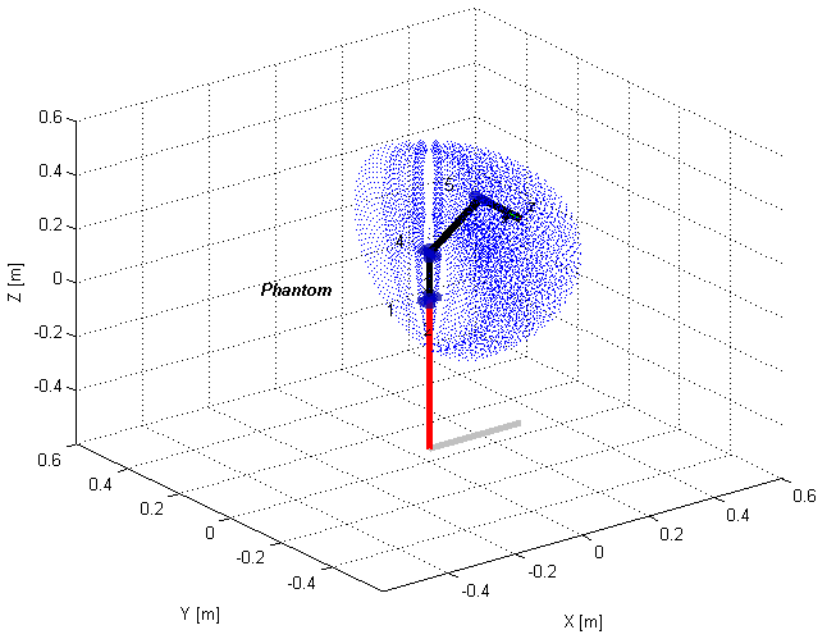

Figure 37. 3D view of the workspace of Phantom Premium 1.5.

Figure 38. Gimbal of the Phantom Premium 1.5 HF.

4.2 First prototype

Based on the initial requirements and experiments with mock-ups, the first prototype was made. It had the kinematic structure with 7 DOF as shown in Figure 39a which shows the similarities to the Phantom Premium in Figure 39b. Table 6 shows the Denavit-Hartenberg parameters of the first prototype. The same analysis (see Appendix B) as with Phantom was performed with the first prototype. There were no kinematic singularities inside the workspace.

Table 6. Denavit-Hartenberg parameters of the first prototype.

i	α_i	a_i	d_i	θ_i
1	- π/2	0	0	q_1
2	- π/2	0	0.1m	q_2
3	π	0.3 m	0	q_3
4	π/2	0	0	q_4
5	π/2	0	0.3 m	q_5
6	- π/2	0	0	q_6
7	0	0	0	q_7

The drum-capstan transmissions were replaced with spur-gear transmission to make the workspace bigger. The gimbal size and the range of angular motions by joints were increased. Placement of control electronics outside the device, gave freedom of placing the device closer to the user. One extra joint was added to the bottom of the device to allow the user to lean forward. This allowed bigger workspace (Figure 40) compared to the Phantom Premium (Figure 37). Figure 41 shows that the workspace forms a large sphere shaped area.

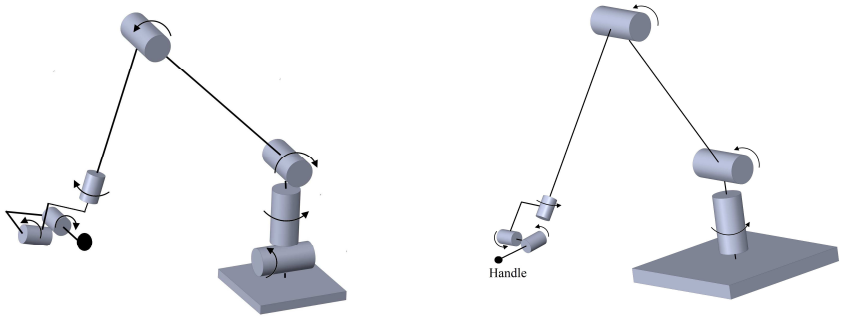

a) b)

Figure 39. Kinematic structure of the a) first prototype and b) the Phantom Premium 1.5 HF.

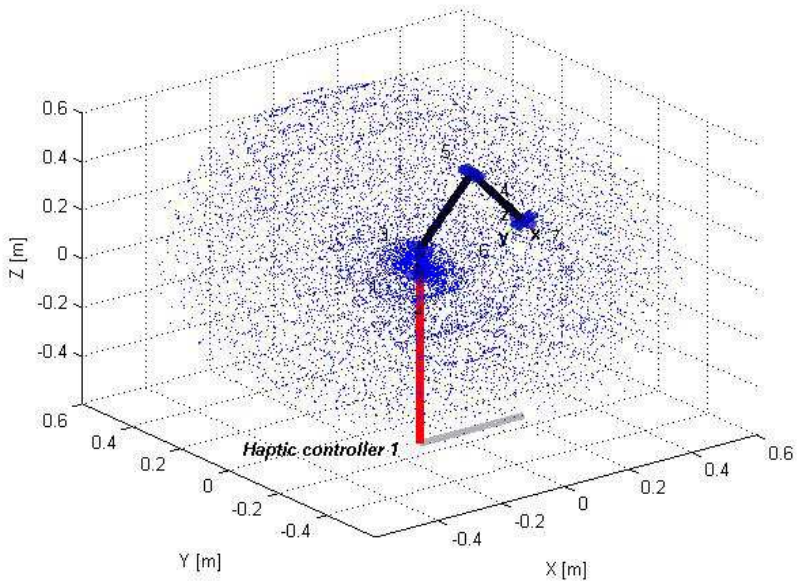

Figure 40. 3D workspace of the first haptic controller prototype

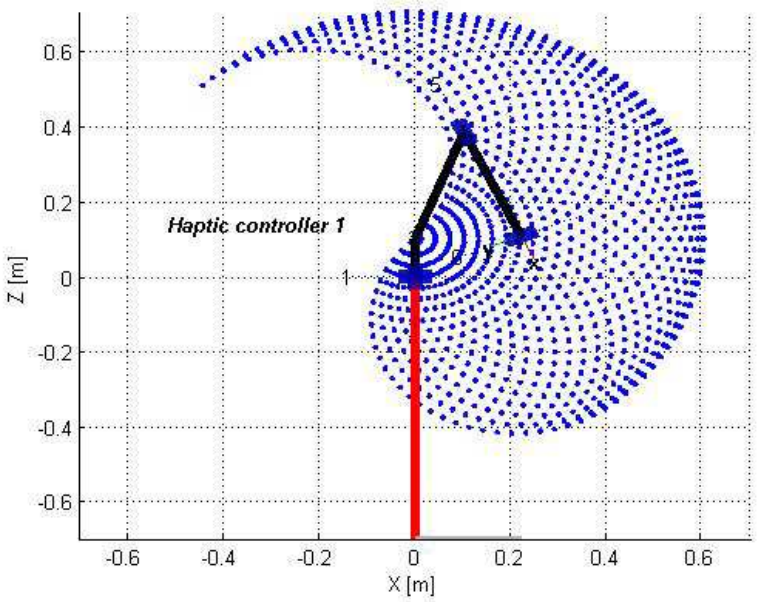

Figure 41. Sliced side view of the workspace of the first haptic controller prototype, joint rotating around Z axis is locked for the image.

Despite the seemingly large workspace, not all orientations and positions could be reached easily by a user, due to singularities in joint extremities. During the testing of the device it sometimes blocked the users view forward. Control motion directions were not clear to the user due to some of the motions occurring as movements of several joints. Using one joint per control direction felt more natural and less confusing as in conventional joystick. This became a new criterion for searching alternative mechanism for a haptic device.

4.3 Second prototype

Based on the requirements formed during testing of the first prototype, the second prototype was built. The idea of a joystick and its clear control directions was used as a beginning of the design. To add more degrees of freedom, it could be attached to the end of a lever with a 2 DOF rotational joint in the other end. The joystick was next replaced with a gimbal. This allows more fluent and natural motion of the users hand independent on the orientation or the location of the controller mechanics. As a result a 6 DOF mechanism in Figure 42 with a workspace shown in Figure 43 was made. Joint 1 provides the backwards and forwards control direction; joint 2 is for the vertical motion and joint 3 is for sideways direction. Joints 4, 5 and 6 provide three rotational control directions. Toolhandle is the point where user holds the controller by hand. Table 7 shows the Denavit-Hartenberg parameters of the second prototype. There were no kinematic singularities inside the workspace based on the analysis shown in Appendix B. Figure 44 shows a sliced side view of the workspace of the second haptic controller prototype. The workspace is hollow inside the torus as the lever between joints 2 and 3 is fixed in length. The width of the torus shape is defined by the distance between the gimbal centre and joint 3.

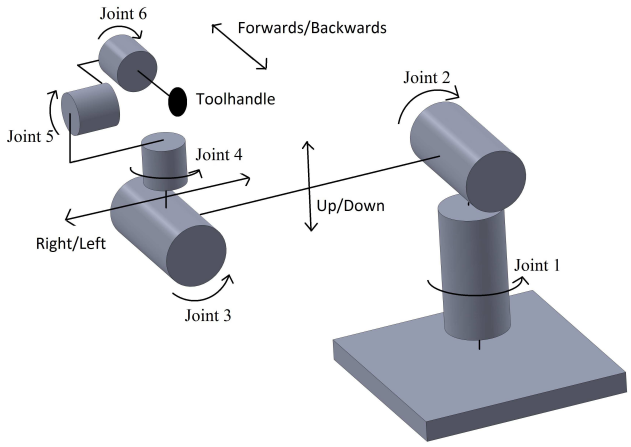

Figure 42. Second haptic controller prototype.

Table 7. Denavit-Hartenberg parameters of the second prototype

i	α_i	a_i	d_i	θ_i
1	- π/2	0	0	q_1
2	π	0.163 m	0	q_2
3	π/2	0	0	q_3
4	π/2	0	0.052 m	q_4
5	π/2	0	0	q_5
6	0	0	0	q_6

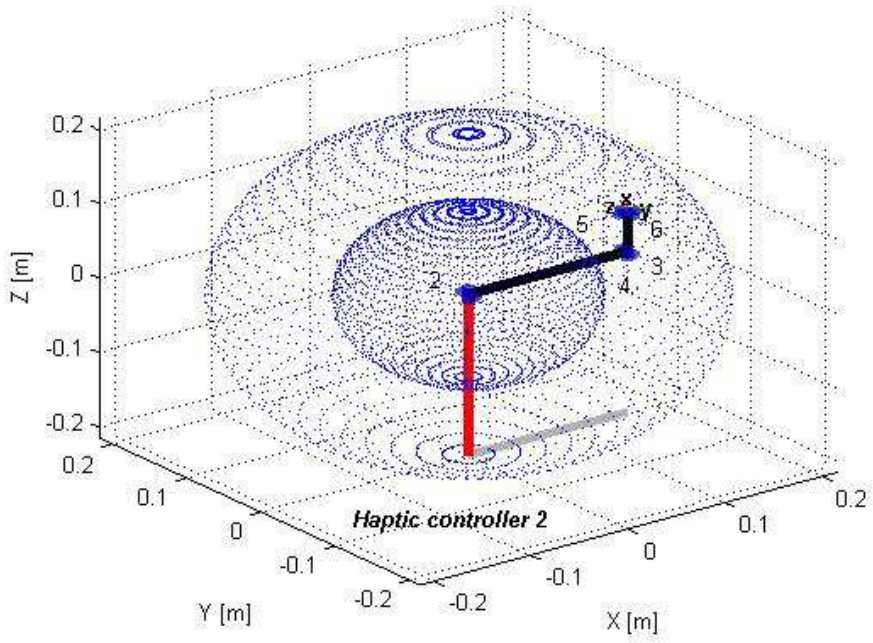

Figure 43. 3D view of the workspace of the second haptic controller prototype.

In Figures 43 and 44 it can be seen that all control directions can be performed in any point of the workspace between the two spherical surfaces.

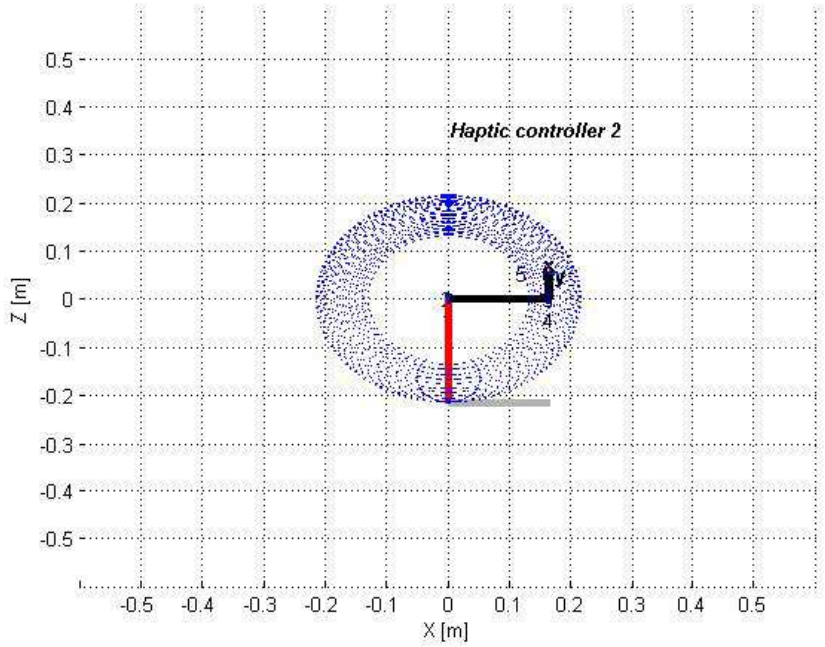

Figure 44. Sliced side view of the workspace of the second haptic controller prototype.

4.4 Realisation of the second prototype

This section describes the hardware, software and force controller of the second prototype of the haptic device (Heikkinen & Handroos, 2013 a).

4.4.1 Hardware

In Figure 42 was shown the kinematic structure of the second prototype of the haptic controller. In Figure 45 is shown a picture of the actual prototype device. The first three joints were realised with Dynamixel EX-106+ servos (Robotis, 2013) with stall torque of 10.5 Nm. Joints 4, 5 and 6 were made with 5 kΩ linear potentiometers. Due to the fragility of the Dynamixel servos, additional load carrying bearings were added to the mechanism. The prototype was made from aluminium to make it lightweight. The mechanical link between joints 2 and 3 was a square aluminium tube of 22 cm and distance between joint 3 and 4 was 2 cm. The gimbal was built from strips of aluminium sheet and attached together with potentiometers.

Toolhandle in the middle of the gimbal is a plastic box as shown in Figure 46. The box contains the following functional buttons:

Dead man's switch: Not pressed, locks all joints in place. When pressed, allows free movement of all joints.

Force/Control mode start button: Enables the force feedback input and control signal output from the device. When Force/Control mode start button is released and again pressed down, the reference values for control are reset to zero.

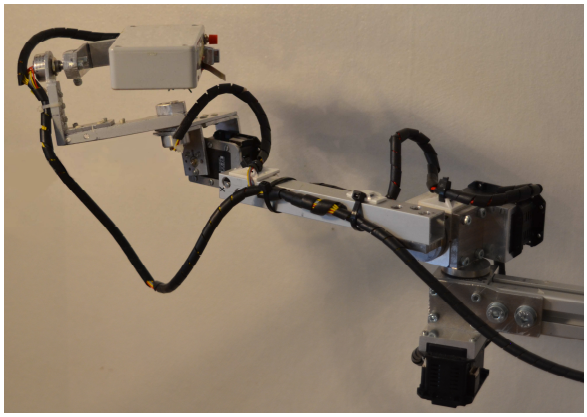

Figure 45. Second prototype mechanism.

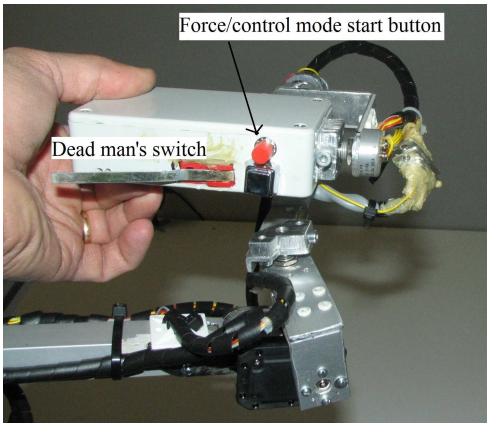

Figure 46. Plastic box as toolhandle.

The computer hardware was divided into two parts (Figure 47) which execute their programs at different speeds and perform separate tasks of the controller functionality.

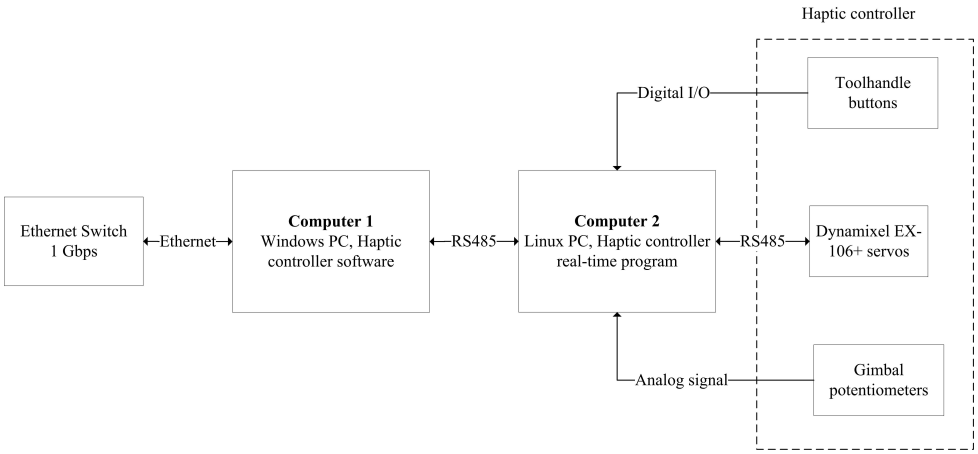

Figure 47. Hardware division of the haptic controller prototype.

The higher speed portion of the controller hardware uses computer 2 with real-time Linux. It is connected to the servos using a 1Mbps half-duplex RS485 connection and to the gimbal potentiometers using an analogue signal connection to an A/D card. The tool handle buttons are connected to a digital I/O card. Connection to computer 1 is with a 2Mbps full duplex RS485. The computer 1 is connected outside with a 1 Gbps Ethernet connection.

4.4.2 **Software**

The programs of the haptic controller shown in Figure 48 were made and debugged with Microsoft Visual Studio (Microsoft, 2012) and Code::Blocks IDE (Free Software Foundation, Inc., 2007).

The real-time program executes as a single thread and functions mostly like haptic rendering described in (Robles-De-La-Torre, 2008). In the beginning, all the servos and other hardware are initialised. The statuses' of the buttons, positions of servos and potentiometer signal values are read. This data is sent to computer 1 (slower Windows program).

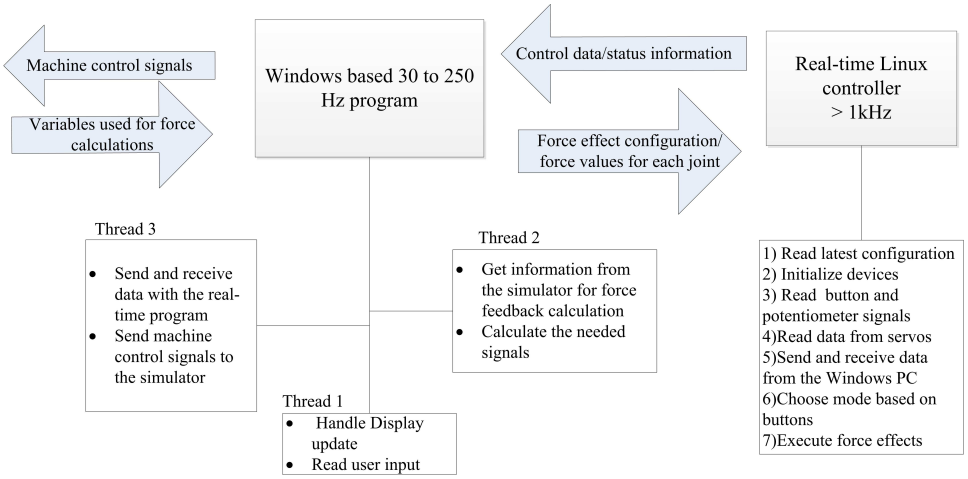

Figure 48. Division of the haptic controller software.

Next the real-time program chooses the mode of operation based on the buttons' states and executes the individual force effects on each joint. The lower speed program in computer 1 is also shown in Figure 48. It has three parallel running threads. The synchronisation of the threads was made as described in subsection 3.1. Also here, problems with synchronisation were not observed.

Thread 1 displays information to the user and reads user input and passes it to the other two threads. Thread 2 collects and calculates information for force feedback and passes it to other threads for further processing. Thread 3 communicates with the real-time program, handles device axis configurations and control and force values.

4.4.3 Force controller

The force controller of the haptic device is a modified version of an open loop impedance controlled system, where the user closes the force loop. A force is generated based on position as an input (Kern, 2009). The open loop impedance control is used mainly with force effects, like virtual walls and axis locks. The virtual walls are made as a ramp of force increasing from the latest force before wall up to specified maximum value as shown in Figure 49. If the servo motor's position is inside the wall, it is driven to the first position outside. Walls are used for limiting the motions of the haptic controller. In Figure 50 is an example of the walls with forwards/backwards as the control direction. If the controller or individual joints need to be locked, the target position is set to the current one with enough torque to prevent forced movements by the user.

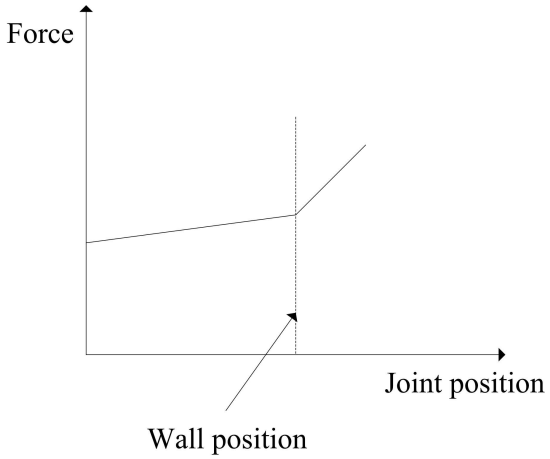

Figure 49. Virtual wall created with force controller.

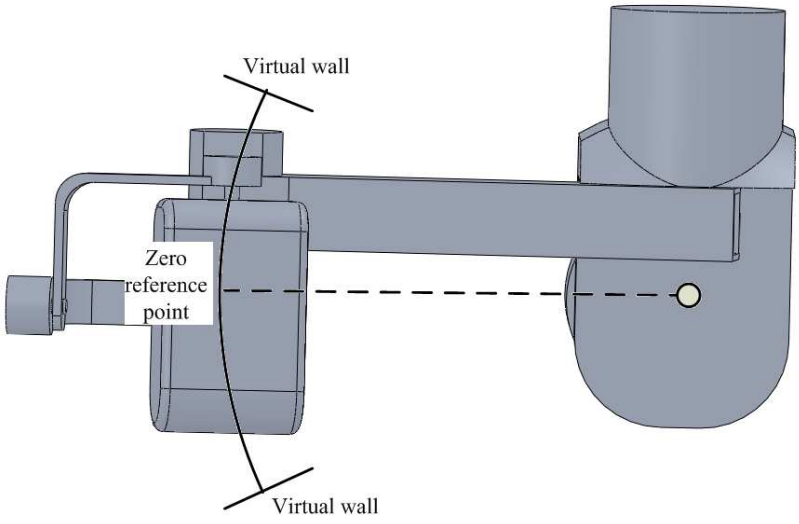

Figure 50. Virtual walls limiting the control motion of forwards-backwards direction.

4.4.4 Performance evaluation of the servos

As there was not enough information available of the used Dynamixel EX-106+ servos (Robotis, 2013), their dynamic performance could not be evaluated properly and were treated mainly as black boxes in the system. Few tests were made with servos to evaluate their performance in a haptic controller. First test created virtual walls of different flexibility to see if the servo could produce the effect without the user feeling any vibrations while holding the controller tool handle. Only in the hardest of surface, some vibration could be felt, but mostly neither the handle nor the controller itself vibrated. Next, changing of force with different ramps was tested and the ramp was felt as smooth without any vibrations or sudden changes. Stickiness effect like a stretching chewing gum was tested also without any vibration or unwanted force feelings. As the effects were felt to be acceptable, the servos were considered sufficient in performance for this prototype.

4.4.5 Forward kinematics

The joint space position signals of the servos are converted into a point on a curve drawn by the motion of the controller (Figures 51 and 52) by using Equation (22).

$$pos_{ctrl}=L\cdot radstep\cdot(pos_{cur} - pos_{zero}), \quad (22)$$

where pos_{ctrl} is the controller position signal, pos_{cur} is the current absolute position of the joint with value between 0 and 4095, pos_{zero} is the absolute position of the joint at zero reference point with a value between 0 and 4095, *radstep* is the amount of radians per increment of one step in the servo's position sensor, L is the distance in meters between the two joints' centres used for calculating the motion. The motion curve in Figure 51 is the similar for both vertical and forwards-backwards motions of the controller.

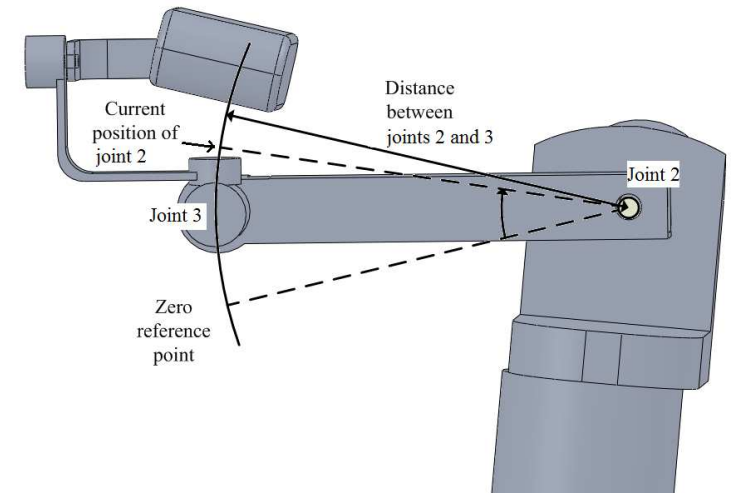

a)

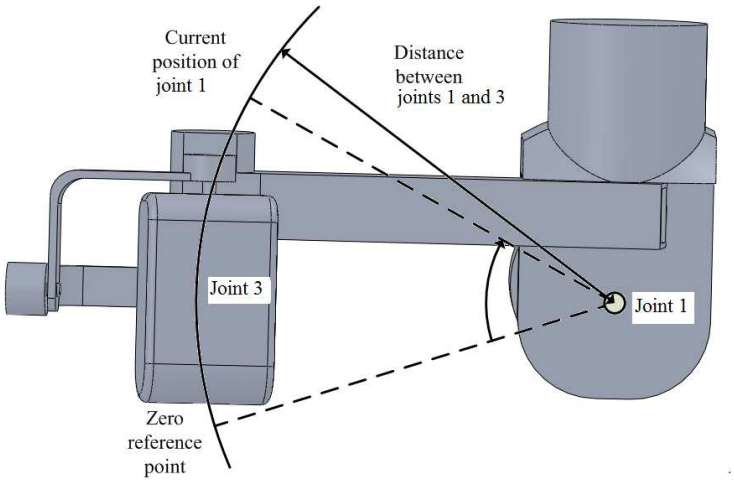

b)

Figure 51. Vertical and forward-backwards motions of the haptic controller: a) side view, b) top view.

The value for L in Equation (22) is the distance between joints 2 and 3 for vertical motion and the distance between joints 1 and 3 for backwards-forwards motion. In Figure 52 is the curved trajectory of the of left-right motion of the controller, where distance L is the distance between joint 3 and the toolhandle.

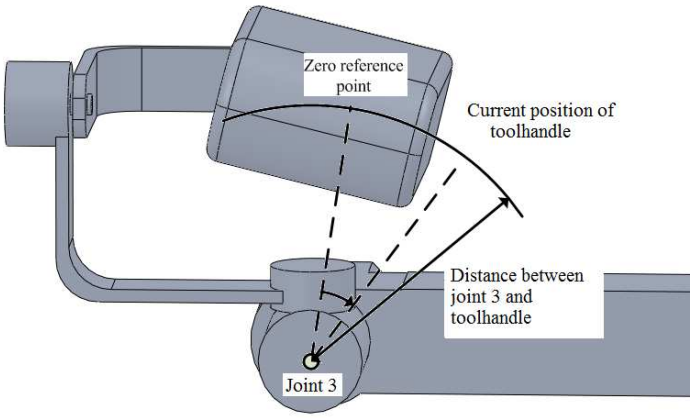

Figure 52. Left-right motion of the haptic controller.

4.5 Comparison with Phantom Premium

Table 8 shows comparison of specifications between Phantom Premium 1.5 HF and the second prototype of the haptic controller.

Table 8. Device specification comparison

Parameter	Phantom Premium 1.5 HF	Second prototype of haptic controller
Nominal Position Resolution	0.007 mm	0.23 mm
Maximum exertable force (nominal position)	37.5 N	-
Continuous exertable force (nominal position)	6.2 N	47.7 N
Force Feedback	x, y, z	x, y, z
Position Sensing	x, y, z (roll, pitch, yaw upon special request)	x, y, z (roll, pitch, yaw)
Interface	Parallel Port	Ethernet/VRPN

The nominal position resolution of the second prototype is much lower than that of Phantom's. However, this design is made specifically for mobile machine control purposes, where resolution requirements are not as strict as, for instance, in medical applications. The force produced by the second prototype is larger than that of Phantom's. It can be concluded that with a further developed prototype, smaller servomotors can be used.

Advantages of the second prototype over Phantom Premium for mobile machine control are:

1. Clear directions of control motions as with joysticks, one joint per direction.

2. Second prototype allows a wide variety of placement positions by the driver's seat.

3. No limitations inside workspace for any control direction.

4. Bigger gimbal to allow use of symbolic tools as a toolhandle.

4.6 User tests

This section contains description of the test setup, test procedure and analysis of results. User tests were organised for investigating the functionality of the second prototype of haptic controller. The task for the test users consisted of operating a rubber tyred gantry (RTG) and stabilising a swinging container. Testing of different force feedback variables for haptic feedback as in (Farkhatdinov & Ryu, 2008) was included. From the tests, also information of the ergonomics of the device, user modifiable settings and instructions for further development were desired.

4.6.1 RTG simulator

The machine model used for the tests was a real-time dynamic model of a RTG. It operates in harbours transferring containers inside the harbour area and placing them in high stacks (Figure 53).

This model has been tested for realism in earlier projects and by the companies using it. Therefore, it is assumed that this model is sufficient for user testing in the VRERS. In machines like RTG and also other overhead cranes, swinging of the load hung from long steel cables can be a problem (Farkhatdinov & Ryu, 2008). A Graphical simplification of the problem can be seen in Figure 54.

As the driver moves the load attached to the cables forwards or backwards, the load can start to swing as shown in the Figure 54. Swinging of the load (container) can be reduced by the driver with normal joysticks without force feedback: either by lifting the load up and shortening the length of the cables or by moving the load back and forth. In a non-force feedback case the driver uses mainly vision to aid in the controlling of the

swing motion. In the haptic controller tests this vision information is combined with force feedback information.

Figure 53. RTG and containers, Copyright © Cargotec Corporation

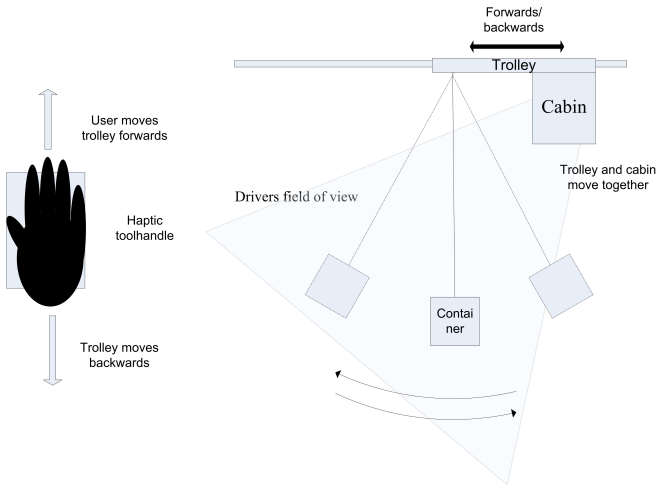

Figure 54. Simplified version of a RTG.

The tested force feedback was given for the backwards and forwards swinging motion using joint 1 (Figure 42) of the controller. Also force feedback was given using joint 2 based on containers up/down motions speed with compensation against gravity. The sideways motion of the RTG was not used as it is too slow for damping swing motion.

The user controlled the containers forwards/backwards and up/down movements with rate mode. The rate control of the RTG was chosen for two reasons: the machine was originally operated with rate control and due to problems with accuracy in position control in a big working area as shown in (Kim, Tendick, Ellis, & Stark, 1987).

4.6.2 Test setup for the haptic controller

The VRERS with Virtools (Dassault Systemes, 2013) used in this test setup was presented in chapter 2 and in (Heikkinen, Luostarinen, & Handroos, 2012). Tests were made without the motion platform, due to the motions of the RTG being relatively small. In the tests all users were using 3D glasses with head tracking and simple machine sounds from the simulator. Dynamics of the RTG were calculated in a separate program by (MeVea Ltd., 2013). In Figure 55 is shown the test system with data flow. Information for the force feedback is read by the controller and converted into torque and position signals to the haptic device. Haptic device imposes a force on the user while the user inputs data into the haptic device as position information. Haptic device transfers position information to the controller which converts it into rate signals for the RTG simulator. VRERS displays user the changes of RTG behaviour. Figure 56 shows a picture of the RTG simulator, driver's seat and the haptic controller prototype.

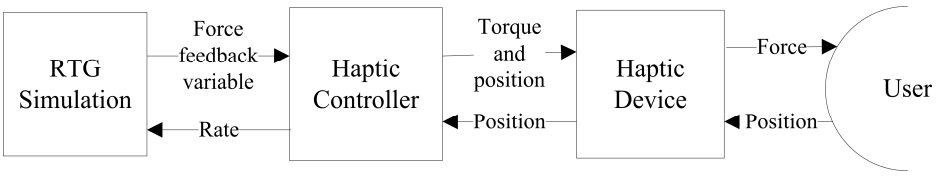

Figure 55. Flow of data in the test setup with RTG simulator.

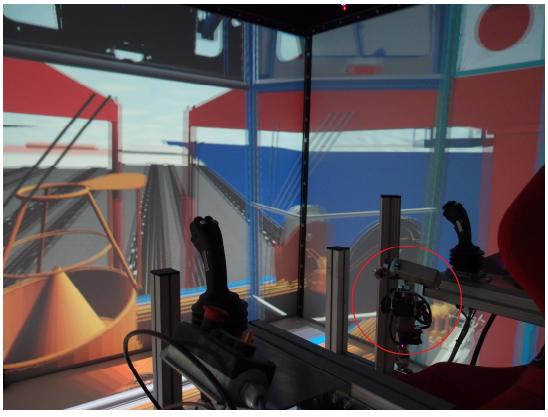

Figure 56. Second prototype of haptic controller (circled in red) with RTG simulation.

4.6.3 Test procedure

Test procedure in short was as follows:

1. Introduction to the RTG simulator, the haptic controller and the task.
2. Practice period and adjustment of force variables.
3. Tests with different sources for force feedback signals.
4. Answering questions of usability of the haptic controller.

In the following the test procedure is elaborated in details. First, the test user was given brief introduction on using RTG and shown example of operation. Next, each user was allowed to drive freely for few minutes to get feeling of the virtual 3D environment and haptic controller.

Task of the user was to stabilise the container swing. The swinging motion of the load was initially caused either by the test subject or the author. Then the user tried to dampen the swinging motion. The settings of each user were set and recorded individually to see what parameters should be user modifiable. The values of minimum and maximum forces used as force feedback was adjusted for each user.

Three different sources for force feedback signals were tested for stabilising the load swing. The used variables were swing angle, swing speed, and a combination of both. Direction of the force feedback was tested for each variable as not inverted and inverted in relation to the direction of motion.

Behaviour of the test subjects was observed during operation of the RTG with the haptic controller. Users were asked general questions regarding the ergonomics and usability of the haptic controller. Feedback was also taken on the controllability of the swing motion. The performance of the haptic controller was measured to see the refresh rates of the different software components.

4.6.4 Test group

Test users with different level of experience and knowledge of virtual reality environments and mobile machines were used in the test. Common factor between users was no previous experience in haptic controllers. The test subjects belonged to the staff of LUT. The test group included 5 people, 1 woman and 4 men, aged between 30 and 60 years. A limiting factor for the choosing of the testers was the secrecy of the development process at the time.

4.7 Results and analysis

This section contains the results and analysis of the user tests made with the haptic controller prototype.

4.7.1 Minimum and maximum forces

Forces applied to the user were linearly scaled between a minimum and maximum value of force. If force value went above or below limits, it was saturated to the equivalent maximum or minimum values. The direction of the force was defined by the sign of the input value.

It was observed that force scaling was similar between all tested individuals. In Table 9 are shown the settings of the user adjusted forces from the tests of forward/backward motion of the haptic controller.

Table 9. Results of force settings for forward/backward motion of the haptic controller.

Percent of maximum torque, [%]	Estimated torque of motor, [Nm]	Estimated force, [N]
0	0	0
1	0.1	0.48
5	0.52	2.38
15	1.58	7.13

The minimum forces used were mostly at 0 N. For some test subjects the minimum force was increased to a value between 0.48 and 2.38 N. Average maximum force that felt comfortable for the users was around 7.13 N and larger forces were only used with virtual walls and locks. The maximum forces applied were sometimes lowered slightly to stop user's arm becoming tired. As the torques used are maximum 15 % of the stall torque of 10.5 Nm of the Dynamixel EX-106+ servos (Robotis, 2013), smaller motors could be used in next prototypes.

4.7.2 Analysis of the force variables

In Figure 57 is shown simplified structure of the RTG. Table shows the different force feedback variables and their behaviour in different parts of the swing motion.

When swing angle is used as a variable, the force is zero when the container is in the middle point of travel or resting in place hanging straight down. Force changes direction depending on the direction the swing takes from the point of zero. Maximum value of force is reached in the extreme point of swing when the swing motion changes its direction.

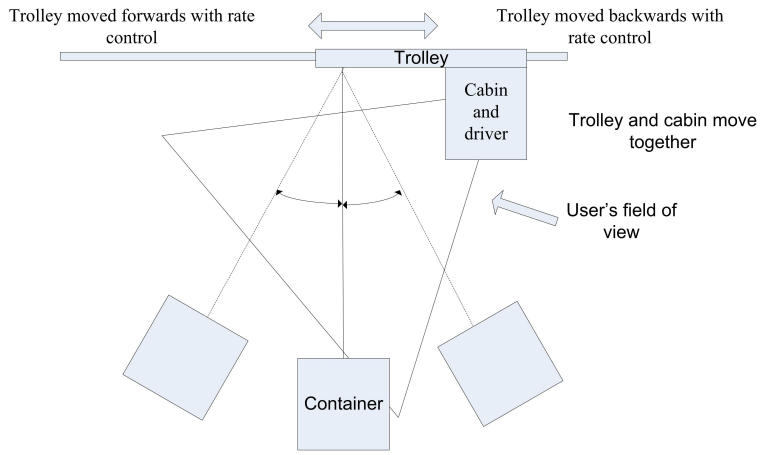

Swing angle	Maximum positive value	0°, changes sign	Maximum negative value
Swing speed	0, changes sign and direction	Maximum value, sign depends on direction	0, changes sign and direction
Combined angle and speed	Maximum value, changes sign	0° value, sign depends on direction of swing	Maximum value, changes sign

Figure 57. Force feedback variables.

With swing speed used as a force variable, maximum value is reached at zero degrees angle when the container is at its lowest point and the cable is hanging straight down. If the container is not swinging, the speed and thus force in this point are zero. Swing speed and the force change their directions and signs at the extreme points of motion, where the container is at its highest point. In these extreme points, the force and speed are momentarily zero.

Combined angle and speed as force feedback variable, was originally made due to noise problems in the speed signal, but were included later because of interest in combining two sensor values together. In this case the absolute maximum value of the force is reached at the extreme point of swing, when the container is at its highest position. The sign and the direction of the force are also changed at this point. Force has a value of zero in the middle of the travel or when the container is at rest. If the container is in motion while passing the zero angle point, the sign is dependent on the direction of the motion.

Results of the tests with the three variables with not inverted and inverted force directions are shown in Table 10. Due to limitations in the simulator, it was impossible to repeat the swinging situation identically every time for comparable data. The situation was considered under control if the oscillating motion in general could be

damped. Situation was considered out of users control if the amplitude of the swing stayed the same or increased despite obvious control efforts by the user.

Table 10. Results of tests with force feedback variables

Variable used for force feedback	Force direction	Results of the user actions
Swing angle	Same as motion	Prevention of swing successful
Swing angle	Opposite to motion	Difficult to control and increased swing
Swing speed	Same as motion	Slowed down and stopped swinging
Swing speed	Opposite to motion	Could not reduce or made swing worse
Combined angle + speed	Same as motion	Slowed down and stopped swinging
Combined angle + speed	Opposite to motion	Could not reduce or made swing worse

When swing angle was used as a force feedback variable with the same direction as the motion, users could control the swing of the container or rather prevent the swing from occurring. After the direction of force was changed opposite to the motion, controlling became difficult and increased the swing.

Swing speed as a variable with the same force direction as the motion, resulted in reduction of the swing and eventually stopping the swinging. After changing the direction of force to be opposite to the motion of the container, users could not control the swing at all and just made the situation worse. However, a few users could after practise control this situation, but not as well as with the non-inverted direction of force.

Combined angle and speed resulted in similar results as the swing speed. With non-inverted direction of the force the users could control the situation and stop the swinging motion of the container. With the inverted force direction, users lost control and made the situation worse.

4.7.3 Observations from the tests

During the user tests, it was observed that the users need to be able to modify several parameters by themselves during the operation of the machine. Adjustments needed were the minimum and maximum forces, offsets and dead zones for forces and control signals. Force scaling should be adjustable at runtime. Offsets and dead zones need to be configured only one time per user.

If the sway angle was in use, the users were all time keeping the force control button pushed and tried to move the container without starting a swing motion. The motions of control seemed continuous and concentrated around the zero point of the controller.

While using the swing speed and combined variables, users released the control button when container changed its direction of swing motion. Release of the button zeroed the control signal going to the RTG. Immediately after which, the button was pushed back down and the controller was moved to opposite direction creating an immediate counter movement to the container swing motion. This behaviour could partly be explained by the human tendency for using bang-bang control as described in (Young & Meiry, 1965). In this case, the bang-bang control was supplemented by the feeling of amount of force and the change of force direction.

It was noticed, with different force variables that the function of stopping a swinging motion and preventing it from even happening are two different things. The angle variable as force feedback signal was best for prevention of swing motion and the two others methods were better for damping an existing motion. Therefore, changing of the feedback signal and control type at runtime might be useful as shown in (Andaluz, Salinas, Roberti, Toibero, & Carelli, 2011).

The inverted force directions of all the three variables were useless and made the control situation difficult. The force variables and their directions should be chosen carefully for each application of the haptic controller.

Big differences in initial skills and learning time were noticed despite all test subjects being beginners. Initially larger forces were used while learning to use the controller. As user became more familiar with the operation of the device and more sensitive to changes in force, value of maximum force was lowered.

The positioning and orientation of the controller were found to be important to the user. Controller should be within a comfortable range of user's body to limit the need of elbows' movement.

If forced movements of the user's hand by the haptic controller are needed, slow speeds with high forces should be preferred. They are felt as a kind of guidance of the hand and don't surprise the user as much as with high speeds.

4.7.4 System dynamic performance

As there was not enough information available for evaluation of the dynamic performance of the used Dynamixel EX-106+ servos, they were considered as “black boxes”. Some tests to verify functionality were made with the servos as explained in subsection 4.4.4.

All refresh rates were measured with self-made programs. Table 11 shows the refresh rates of the system.

Table 11. Refresh rates of the system.

Components	Refresh rate [Hz]
Windows based program of the haptic controller	250
Connection to VRERS	60 - 80
Real-time Linux program of the haptic controller	1000
Real-time simulator	50 - 100

The real-time Linux portion of the haptic controller executed its force control loop at an average of 1 kHz rate. The refresh rate of the Windows based program of the haptic controller was around 250 Hz. The refresh rate towards the VRERS was between 60-80 Hz and the real-time simulator was running at rate between 50-100 Hz. Human skin’s feeling of forces is in frequencies from 10 Hz to 1 kHz and higher and the positional perception of human limbs is from static to 10 Hz (Kern, 2009) (Robles-De-La-Torre, 2008). As the frequency of the real-time Linux force controller was in the range of those defined for human tactile and kinaesthetic perception, the prototype can considered functional.

5 Conclusions

In this chapter the main results of this work are summarised and suggestions for future research are given.

5.1 Key results of the work

Virtual Reality Environment with Real-Time Simulator (VRERS) with a mobile working machine model was designed and built at Lappeenranta University of Technology (LUT), Laboratory of Intelligent Machines. The structure of the VRERS and its software and hardware components are described in details. The advanced VRERS developed includes physically adequate multi body model of a rubber tyre gantry crane (RTG) with real-time solver, four 3-D projected screens, a 6-DOF motion platform and a head tracker. It was assumed in the research that the VRERS gives a sufficiently realistic feeling to the operator of the RTG for making at least comparisons between alternative force variables. The environment was used to test a haptic controller for the control of a mobile working machine.

The usability of a commercially available haptic device Phantom Premium 1.5 HF for mobile machine control application was found to be limited. An electronics box underneath the device restricted the possibilities of placement by the driver's seat and limited the working area of the device. The mechanism often disturbed the user's view to the VRERS. Control motions that were usable in the middle of the device workspace became impossible in the extremities. Therefore, users were limited to starting control motions only from the middle of the working space. Also the gimbal of the Phantom Premium 1.5 HF was too small inside to fit the user's hand with a tool handle. Due to these reasons two alternative haptic mechanisms were proposed. Mechanisms of the Phantom Premium 1.5 HF and two alternative haptic controllers were analysed with Matlab and Robotics Toolbox. The presence of kinematic singularities of the mechanisms was evaluated with the rank of their Jacobian matrixes. All the three choices were found to have kinematic singularities only in their workspace boundaries.

The first alternative prototype had kinematics very similar to the Phantom Premium. Despite the larger workspace than Phantom's, not all orientations and positions could be reached easily by a user, due singularities in joint extremities. Also the users view to VRERS was again often disturbed. The control of motion directions were not clear to the user due to some of the motions occurring as combinations of movements by several joints. Using one joint per control direction, as with a joystick, was found to be more natural and less confusing to use. Instead of using Cartesian space, the haptic feedback was created in the joint space by applying tangential forces.

Based on the observations during testing of the first prototype, a second prototype was built. Its kinematic structure was different from the Phantom and the first prototype. There was only one joint/motor per control direction: one for vertical, horizontal and

forwards/backwards motions each. Also a bigger gimbal was implemented into the design. The nominal position resolution of the second prototype was lower than that of Phantom's. However, this design was made specifically for mobile machine control purposes, where resolution requirements are not as strict as for instance in medical applications. Therefore, resolution was found to be sufficient. The maximum forces produced by the second prototype were larger than that of Phantom's.

User tests were organised for investigating the functionality of the second prototype of haptic controller. The task for the test users consisted of operating a RTG and stabilising a swinging container using visual and haptic information. The RTG was controlled in the rate mode and the force feedback signals formed from alternative variables were tested. The used variables were swing angle, swing speed, and a combination of both with non-inverted and inverted direction of force. It was noticed; with different force variables that the function of stopping a swinging motion and preventing it from even happening are two separate issues. While constructing the force feedback from the swing angle the users could prevent the occurring of swinging motion rather than stop it. The swing speed and combination variable as force feedback signals were better for stabilising an existing swing motion. In all cases, if force direction was inverted to be against the swing motion direction, users lost control of the situation and usually just increased the swing.

Big differences in initial skills and learning time were noticed despite all test persons being beginners. As the user became more familiar with the operation of the device and more sensitive to changes in force, value of maximum force was lowered. The positioning and orientation of the controller were found to be important to the user.

The control loop execution rates of the haptic controllers programs were measured. As the frequency of the real-time Linux force controller was in the range of frequencies defined for human tactile and kinaesthetic perception, the haptic controller's controller functionality division can be seen as a functional solution.

A proposed hardware-in-the-loop (HIL) setup using a motor/generator for emulating the behaviour of a hydraulic pump in an electro-hydraulic hybrid transmissions system was created and tested. The setup consisted of a real-time simulator, two electric motors coupled mechanically together and two frequency converters. The real-time simulator was used for simulating the hydraulic and mechanical parts of a machine. The hydraulic pump emulator consisted of an electric motor and a frequency converter and its control signals were obtained from the real-time simulator. The emulator was seen as a load by the tested electric drive. A real-time model of a hydraulic boom was used in this project. Reference data for comparison was obtained from measurements of a project of a real electro-hydraulic forklift. According to recorded data from the frequency converters, the system behaved as expected and the event recordings were synchronous to each other. When comparing the reference data from the hydraulic forklift setup to the measured data, they both showed the similar behaviour in all used motions.

Two initial criteria were found important for choosing an electric motor to be an emulator of a hydraulic pump in a HIL-setup. First criterion was the dynamic performance of the electric motor in torque control. The second criterion was the pressure/flowrate curve of the emulator electric motor in relation to pump specifications of the simulated hydraulic circuit. An analysis based on the two criteria of choosing a suitable electric motor for emulation was made.

The dynamics for three electrical motors selected were evaluated based on the settling time of step response analysis. The open-loop transfer functions for step response analysis were derived from a simplified model of a torque controlled permanent magnet servomotor. By using limit value theorem it was shown that in torque controlled pump emulator the dynamic properties of the motor are fully dominated by the electrical time constant, while the mechanical time constant can be neglected. The analysis of the refresh frequencies of components in the HIL setup showed that though the used motor was much slower than most components of the setup, the slower rate of the graphics as a source of information guaranteed that the system functioned sufficiently from the human point of view.

An analysis of three electric motors for use as an emulator based on their pressure/flowrate curves was made. Guidance on choosing a suitable electric motor based on dynamic analysis and static performance curves was given. In spite of the finding that the tested electric motors were not ultimate solutions for emulating a hydraulic pump in the application studied, they appeared to provide sufficient static and dynamic capabilities for realistic tests of hybrid electric drives directly driving a hydraulic pump.

5.2 Suggestions for future research

Further research and development of the haptic controller should be made. Other mobile working machines besides the RTG should be tested with it and on larger scale. A new motor and servo controller should be designed specifically for force feedback use. Additional user tests should be carried out with the haptic controller using professional drivers to compare the performance and energy efficiency between a conventional joystick and a haptic controller. Research to find a suitable electric motor for emulating a hydraulic pump should be made.

References

ABB. (2013). *Motion Control program Firmware ACSM1*. Retrieved from http://www.abb.com

Ahlawat, R., Jiang, S., Medonza, D., & Smith, M. H. (2012). On emulating engine and vehicle transient loads for transmission-in-the-loop experiments. *Mechatronics*, 989-996.

Airila, M., Ekman, K., Hautala, P., Kivioja, S., Kleimola, M., Martikka, H., . . . Välimaa, V. (1995). *Koneenosien suunnittelu.* Helsinki: Werner Söderström Osakeyhtiö.

Andaluz, V. H., Salinas, L., Roberti, F., Toibero, J. M., & Carelli, R. (2011). Switching control signal for bilateral tele-operation of a mobile manipulator. *9th IEEE International Conference on Control and Automation (ICCA)* (pp. 778,783). IEEE.

Bauer, M. D., & Rosen, D. W. (1997). An approach to integrated product/process design. *Proceedings of DETC'97 1997 ASME Design Engineering Technical Conferences.* Sacramento, California: ASME.

Butterfly Haptics. (2013). Retrieved from http://butterflyhaptics.com/products/

Corke, P. (2013). *Robotics Toolbox*. Retrieved from Robotics Toolbox: petercorke.com/Robotics_Toolbox.html

Da-Lite. (2013). *Ultra Wide Angle rear projection screen.* Retrieved from http://www.da-lite.com/

Dassault Systemes. (2013). Retrieved from http://www.3ds.com

Donelan, P. (2010). Kinematic Singularities of Robot Manipulators. In E. Hall, *Advances in Robot Manipulators* (pp. 401-415). InTech.

Driscoll, S. (2005). *The Design and Qualification of a Hydraulic Hardware-in-the-Loop Simulator.* School of Mechanical Engineering, Georgia Institute of Technology.

Eckerle Industrie-Elektronik GmbH. (2013). *Eckerle mobile hydraulics*. Retrieved from Eckerle Hydraulics: http://www.eckerle.com/index.php/high-pressure-internal-gear-pumps.html

Elton, M. D., Enes, A. R., & Book, W. J. (2009). A Virtual Reality Operator Interface Station with Hydraulic Hardware-in-the-Loop Simulation for Prototyping Excavator Control Systems. *IEEE/ASME International Conference on Advanced Intelligent Mechatronics.* Singapore: IEEE.

Enes, A. R., & Book, W. J. (2008). A hardware-in-the-loop simulation testbed for emulating hydraulic loads representing the complete dig cycle of a construction machine. *Proceedings of IMECE2008, ASME International Mechanical Engineering Congress and Exposition.* Boston, Massachusetts, USA: ASME.

Enigk, H., Foehl, U., & Wagner, V. (2008). Haptics research at Daimler AG. In M. Grunwald (Ed.), *Human Haptic Perception: Basics and Applications.* Basel – Boston – Berlin: Birkhäuser Verlag.

Farkhatdinov, I., & Ryu, J.-H. (2008). A Study on the Role of Force Feedback for Teleoperation of Industrial Overhead Crane. *EuroHaptics '08 Proceedings of the 6th international conference on Haptics: Perception, Devices and Scenarios* (pp. 796-805). Heidelberg: Springer-Verlag Berlin.

Force Dimension. (2013). *Force Dimension*. Retrieved from Force Dimension Haptics: http://www.forcedimension.com/

Franklin, G. F., J, P. D., & Emami-Naeini, A. (1986). *Feedback Control of Dynamic Systems.* New Jersey: Prentice Hall.

Free Software Foundation, Inc. (2007). *Code::Blocks.* Retrieved from The open source, cross platform, free C++ IDE. : http://www.codeblocks.org

Geomagic. (2013). *Phantom haptic devices*. Retrieved from Geomagic: http://geomagic.com/

Gibson, J. J., & Crooks, L. E. (1938, July). A Theoretical Field-Analysis of Automobile-Driving. *The American Journal of Psychology, 51*(3), 453-471.

Guerrier, P. K., & Edge, K. A. (2001). Hydraulic emulation of injection moulding. *ASME International Mechanical Engineering Congress and Exposition.* New York, NY, USA: ASME.

Hayn, H., & Schwarzmann, D. (2009). Control Concept for a Hydraulic Mobile Machine Using a Haptic Operating Device. *ACHI '09 Second International Conferences on Advances in Computer Human Interactions.*

Heikkinen, J. (2009). Integration of Real-Time Simulator, Motion Platform and Haptics. *Master's Thesis*. Lappeenranta, Finland: Lappeenranta University of Technology.

Heikkinen, J., & Handroos, H. (2013 a). Haptic Controller for Mobile Machine Teleoperation. *The International Review of Automatic Control*, Vol. 6 N 3.

Heikkinen, J., & Handroos, H. (2013 b). Design of a Human Machine Interface for a Mobile Machine using Simulation in Virtual Reality Environment. *International Review on Modelling and Simulations (IREMOS)*.

Heikkinen, J., Luostarinen, L., & Handroos, H. (2012). Virtual environment for investigating Human Machine Interface in Machines with hydraulic transmissions. *Proceedings of The 7th FPNI PhD Symposium on Fluid Power.* Reggio-Emilia.

Heikkinen, J., Minav, T., Handroos, H., & Pyrhönen, J. (2012). Real-time HIL-simulation for testing of electric motor drives emulating hydraulic systems. *International Review of Electrical Engineering (IREE)*.

Hu, Y. (2009). Kinematics and Dynamics of a Master Manipulator. *Modern Applied Science*, Vol. 3, No. 3.

InMotion Simulation. (2013). Retrieved from http://www.inmotionsimulation.com

Jiao, Z., Gao, J., Hua, Q., & Wang, S. (2004). The Velocity Synchronizing Control on the Electro-Hydraulic Load Simulator. *Chinese journal of aeronautics*, 39-46.

Kallmann, M., Lemoine, P., Thalmann, D., Cordier, F., Magnenat-Thalmann, N., Ruspa, C., & Quattrocolo, S. (2003). Immersive vehicle simulators for prototyping, training and ergonomics. *Computer Graphics International, 2003. Proceedings* (pp. 90-95). IEEE.

Karkee, M., Steward, B. L., Kelkar, A. G., & Kemp II, Z. T. (2011). Modeling and real-time simulation architectures for virtual prototyping of off-road vehicles. *Virtual Reality Vol. 15 Issue 1*, 83-96.

Kern, D.-I. T. (2009). *Engineering Haptic Devices: A Beginner's Guide for Engineers.* (D.-I. T. Kern, Ed.) Heidelberg: Springer-Verlag Berlin.

Kim, D., Won Oh, K., Hong, D., Park, J.-H., & Hong, S.-H. (2008). Remote control of excavator with designed haptic device. *ICCAS 2008 International Conference on Automation and Systems.*

Kim, W. S., Tendick, F., Ellis, S. R., & Stark, L. W. (1987). A comparison of position and rate control for telemanipulations with consideration of manipulator system dynamics. *IEEE Journal of Robotics and Automation*, 426-436.

Korkealaakso, P. M., Rouvinen, A. J., Moisio, S. M., & Peusaari, J. K. (2007). Development of a real-time simulation environment. *Multibody System Dynamics*, 177-194.

Kővári, A. (2010). Real-Time Modeling of an Electro-hydraulic Servo System. *Computational Intelligence in Engineering*, 301-311.

Kuusisto, J., Ellman, A., Kaapu, T., & Tiainen, T. (2011). Effect of the immersion level of a virtual loader simulator on the sense of presence. *Proceedings of the ASME 2011 World Conference on Innovative Virtual Reality WINVR2011*. Milan, Italy: ASME.

Kuusisto, J., Kaapu, T., Ellman, A., & Tiainen, T. (2012). Developing VIP2M: a virtual environment for prototyping mobile work machines. *International design conference - DESIGN 2012*. Dubrovnik - Croatia.

Leitner, J. (1996). Space technology transition using hardware in the loop simulation. *Aerospace Applications Conference, 1996. Proceedings.* (pp. vol.2, pp.303,311 vol.2, 3-10). Aspen, USA: IEEE.

Lozoya-Santos, J. d., Tudon-Martinez, J. C., Morales-Menendez, R., & Ramirez-Mendoza, R. (2012). Comparison of On-Off Control Strategies for a Semi-Active Automotive Suspension using HiL. *Latin America Transactions, IEEE*, Vol.10 , N.5, 2045 - 2052 .

Merritt, H. E. (1967). *Hydraulic Control Systems.* New York: John Wiley & Sons.

MeVea Ltd. (2013). Retrieved from http://www.mevea.com

Microsoft. (2012). *Visual Studio*. Retrieved from http://www.microsoft.com/visualstudio/

Minav, T. (2011). Electric-drive-based control and electric energy regeneration in a hydraulic system. *Doctoral thesis*. Lappeenranta, Finland: Lappeenranta University of Technology.

Montonen, J., Montonen, J.-H., Immonen, P., Murashko, K., Ponomarev, P., Lindh, T., . . . Pyrhönen, J. (2012). Electric Drive Dimensioning for a Hybrid Working Machine by Using Virtual Prototyping. *Proceedings of the IX International Conference on Electrical Machines 2012* (pp. 921-927). Marseille, France: IEEE.

Naturalpoint, Inc. (2013). *Optitrack and Tracking Tools*. Retrieved from http://www.naturalpoint.com/optitrack/

Nitsch, V., & Färber, B. (2012). A Meta-Analysis of the Effects of Haptic Interfaces on Task Performance with Teleoperation Systems. *IEEE Transactions on Haptics*.

NovintFalcon. (2013). Retrieved from http://www.novint.com/index.php/products/novintfalcon

NVIDIA Corporation. (2013, February). *NVidia 3D Vision Pro glasses*. Retrieved from http://www.nvidia.com/object/3d-vision-professional-users.html

Parker, N. R., Salcudean, S. E., & Lawrence, P. D. (1993). Application of force feedback to heavy duty hydraulic machines. *Proceedings IEEE International Conference on Robotics and Automation.*

Peternier, A., Cardin, S., Vexo, F., & Thalmann, D. (2007). Practical Design and Implementation of a CAVE Environment. *Proceedings 2nd International Conference on Computer Graphics Theory*, (pp. 129-136).

Petersheim, M. D., & Brennan, S. N. (2008). Scaling of hybrid electric vehicle powertrain components for hardware-in-the-loop simulation. *IEEE International Conference on Control Applications* (pp. 720–726). IEEE.

Ramadoss, L., & Hung, J. Y. (2008). A study on universal serial bus latency in a real-time control system. *Industrial Electronics, 2008. IECON 2008. 34th Annual Conference of IEEE* (pp. 67-72). IEEE.

Robles-De-La-Torre, G. (2008). Principles of haptic perception in virtual environments. In E. Grunwald, *Human Haptic Perception* (pp. 363-379). Birkhäuser Verlag.

Robotis. (2013, February). *Dynamixel EX-106+ servo datasheet.* Retrieved from http://www.robotis.com

Ryu, J., Chun, J., Park, G., Choi, S., & Han, S. H. (2010, April-June). Vibrotactile Feedback for Information Delivery in the Vehicle. *IEEE Transactions on Haptics, 3*(2), 138-149.

Saat, R. (2012). Retrieved from Free Windows Modbus Master: http://mbserver.tripod.com/

Sarikhani, A., & Mohammed, O. A. (2012). HIL-Based Finite-Element Design Optimization Process for the Computational Prototyping of Electric Motor Drives. *IEEE Transactions on Energy Conversion*, Vol. 27 , N. 3, 737 - 746.

Shiong, C. Y., Jalil, M., & Hussein, M. (2009). Motion visualisation and control of a driving simulator motion platform. *Proceedings of an international symposium: Mechatronics and its Applications.*

Sinha, R., Liang, V. C., Paredis, C. J., & Khosla, P. K. (2001). Modeling and Simulation Methods for Design of Engineering Systems. *Journal of Computing and Information Science in Engineering*, Vol. 1, pp. 84-91.

Takemoto, A., Yano, K., Miyoshi, T., & Terashima, K. (2004). Operation assist control system of rotary crane using proposed haptic joystick as man-machine interface.

Robot and Human Interactive Communication,13th IEEE International Workshop.

The Guitammer Company. (2013). *ButtKicker, Low frequency audio transducers.* Retrieved from http://www.thebuttkicker.com/

Timmermans, J. M., Van Mierlo, J., Lataire, P., Van Mulders, F., & McCaffree, Z. (2007). Test Platform for Hybrid Electric Power Systems: Development of a HIL Test platform. *European Conference on Power Electronics and Applications* (pp. 1-7). Aalborg : IEEE.

Trigui, R., Jeanneret, B., Malaquin, B. F., & Plasse, C. (2007). Hardware In the Loop Simulation of a Diesel Parallel Mild-Hybrid Electric Vehicle. *Vehicle Power and Propulsion Conference, VPPC* (pp. 448 - 455). Arlington, TX, USA: IEEE.

Viewsonic. (2013). Retrieved from Viewsonic projectors: http://www.viewsoniceurope.com

Viitaniemi, J., Aromaa, S., Leino, S.-P., Kiviranta, S., & Helin, K. (2010). *Integration of User-Centred Design and Product Development Process within a Virtual Environment.* VTT. Tampere: VTT. Retrieved from http://www.vtt.fi/publications/index.jsp

Villaverde, A. F., Raimúndez, C., & Barreiro, A. (2012). Passive internet-based crane teleoperation with haptic aids. *International Journal of Control, Automation and Systems*, Vol 10, Issue 1, pp 78-87.

VRPN. (2013). Retrieved from Virtual Reality Peripheral Network: http://www.cs.unc.edu/Research/vrpn/

Wildenbeest, J., Abbink, D., Heemskerk, C., van der Helm, F., & Boessenkool, H. (2012). The Impact of Haptic Feedback Quality on the Performance of Teleoperated Assembly Tasks. *IEEE Transactions on Haptics.*

Xiaochen, Y. (2011). Virtual Reality Environment For Development and Simulation of Mobile Machine. *Master's Thesis.* Tampere: Tampere University Of Technology.

Young, L. R., & Meiry, J. L. (1965). Bang-Bang Aspects of Manual Control in High-Order Systems. *IEEE Transactions on Automatic Control.*

Yousefi, H., Handroos, H., & Soleimani, A. (2010). Usability test in a virtual environment: a case study based on a mining machine. *ASME 2010 10th Biennial Conference on Engineering Systems Design and Analysis, ESDA2010* (pp. 603-611). Istanbul, Turkey: ASME.

Yousefi, H., Soleimani, A. M., & Handroos, H. (2009). Human Centered Design of Mobile Machines by a Virtual Environment. *Human Centered Design: First International Conference, HCD 2009.* San Diego, CA, USA: Springer.

APPENDIX A: Bode plots and bandwidth of electric motors

Bandwidth from Matlab for electric motor MS4813:

fb_ms4813=bandwidth(TF_ms4813) %in radians/second

fb_ms4813 = 262.5338

Bode diagram for electric motor MS4813:

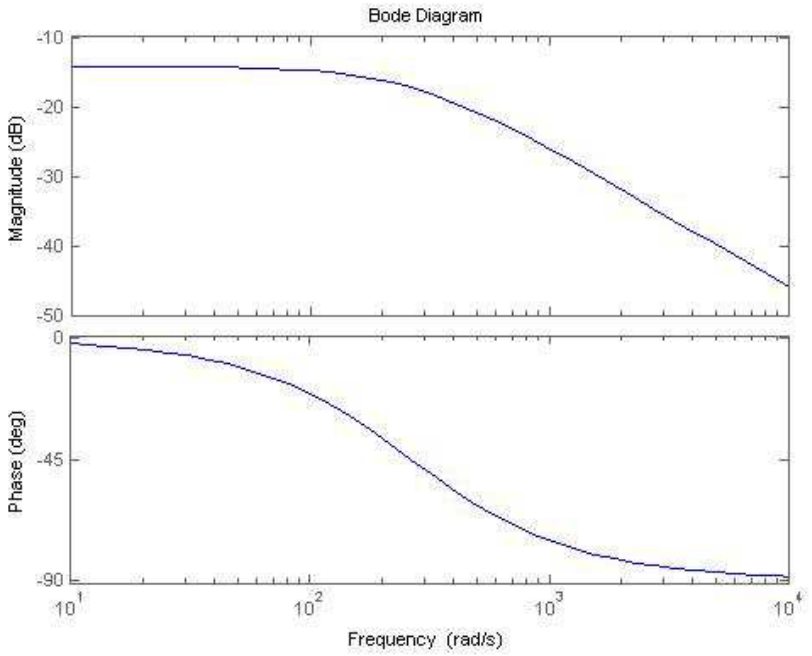

Bandwidth from Matlab for electric motor MS4889:

fb_ms4889=bandwidth(TF_ms4889) %in radians/second

fb_ms4889 = 70.2555

Bode diagram for electric motor MS4889:

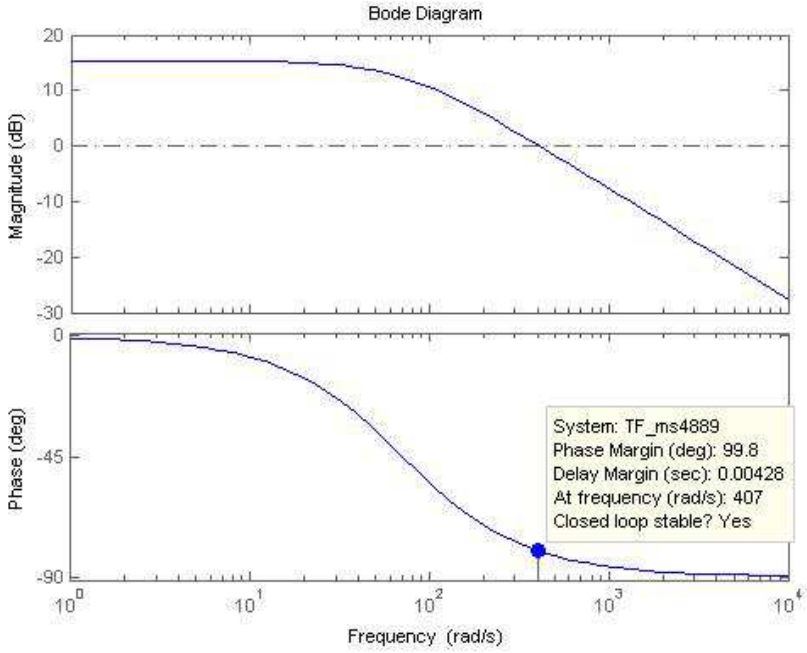

Bandwidth from Matlab for electric motor BLS-144:

>> fb_bls144=bandwidth(TF_bls144) %in radians/second

fb_bls144 = 226.7337

Bode diagram for electric motor BLS-144:

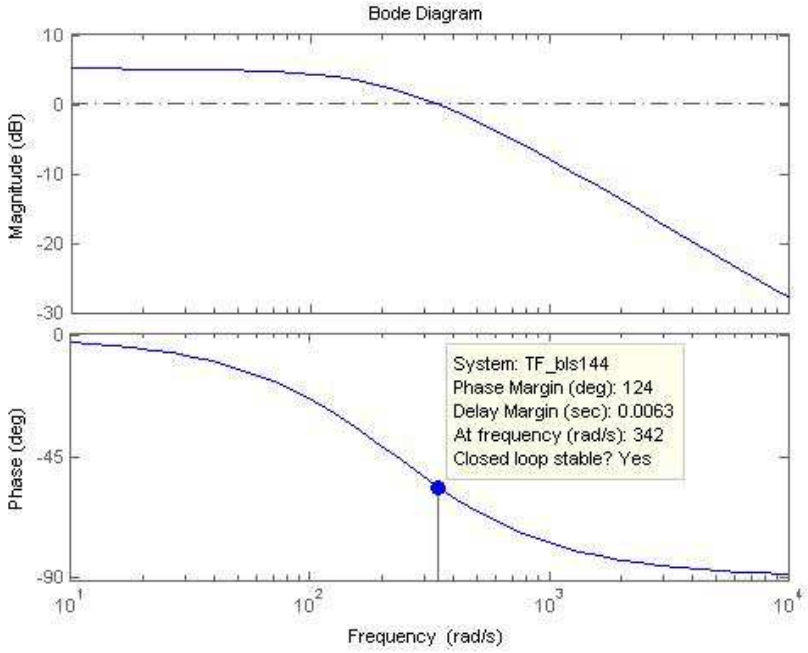

APPENDIX B: Robotics toolbox/Matlab code for kinematic analysis

PHANTOM PREMIUIM 1.5 HF

```
DHPHANTOM_MOD=[0,0,0,-pi/2;0,0.17,0,0;0,0,0,pi/2;0,0,0.215,0;0,0,0.17,-pi/2];

RPHANTOM_MOD=SerialLink(DHPHANTOM_MOD);

% change the joint limits of RPHANTOM_MOD to

[-pi,pi;-pi/2,pi/2;-1.396,1.7453;-1.3962,1.396;-pi,pi]

%change the RHPHANTOM_MOD joint offsets to the following

[-pi/2,0,0,-pi/2,pi/2]

%set the hartenberg variable mdh from the RHPHANTOM_MOD table to 1 for
%modified Denavit-Hartenberg version

%set the base to following matrix for correct orientation

[0,0,1,0;1,0,0,0;0,1,0,0;0,0,0,1]

% generating symbolic math object of phantom premium 1.5

cGenPHANTOM_MOD=CodeGenerator(RPHANTOM_MOD);

% creating the symbolic forward kinematic matrix

TPHANTOM_MOD=cGenPHANTOM_MOD.genfkine();

% creating the symbolic jacobian matrix

j0PHANTOM_MOD=cGenPHANTOM_MOD.genjacobian();

%Calculation of rank and size of Jacobian matrix

rank(j0PHANTOM_MOD)

size(j0PHANTOM_MOD)

%calculating numerically the rank of the Jacobian matrix by cycling through selection
of angles of joints j1, j2 and j3 using the following command

rankk=rank(RPHANTOM_MOD.jacob0([0,j1,j2,j3,0]));
```

1st prototype

DH1STPROTO=[0,0,0,-pi/2;0,0.1,0,-pi/2;0,0,0.3,pi;0,0,0,pi/2;0,0.3,0,pi/2;0,0,0,-pi/2;0,0,0,0];

R1STPROTO=SerialLink(DH1STPROTO);

% change the joint offset matrix in object R1STPROTO from [0,0,0,0,0,0,0] to [pi,pi/2,pi,pi/2,-pi/2,pi/2,0] to orient the device properly

% change base matrix to [0,0,1,0;-1,0,0,0;0,-1,0,0;0,0,0,1] to orient the device

% joint 7 is for the end effector

cGen1STPROTO=CodeGenerator(R1STPROTO);

%create the symbolic version of device

T1STPROTO=cGen1STPROTO.genfkine();

%create symbolic forward kinematics matrix

j01STPROTO=cGen1STPROTO.genjacobian();

%created the jacobian matric for the 1st prototype

%Calculation of rank and size of Jacobian matrix

rank(j01STPROTO)

size(j01STPROTO)

%calculating numerically the rank of the Jacobian matrix by cycling through selection of angles of joints j2, j3, j4 and j5 using the following command

rank=rank(R1STPROTO.jacob0([j2,j3,j4,j5,0,0,0]));

2ND PROTOTYPE

```
DH2NDPROTO=[0,0,0,-pi/2;0,0,0.1630,pi;0,0,0,pi/2;0,0.052,0,pi/2;0,0,0,pi/2;0,0,0,0];

R2NDPROTO=SerialLink(DH2NDPROTO);

%set the joint offsets in the    R2NDPROTO object from [0,0,0,0,0,0] to

[-pi,pi,0,pi/2,pi/2,0] to orient the haptic controller properly

%last joint is the end effector

% change limits of joints to [–pi,pi;-pi/2,pi;-pi/4,-1.25*pi;-pi/2,pi/2;-pi/4,pi/4; -pi/4,pi/4]

cGen2NDPROTO=CodeGenerator(R2NDPROTO);

 %generate symbolic object of the robot

T2NDPROTO=cGen2NDPROTO.genfkine();

 %generate symbolic forward kinematics matrix of the 2nd prototype

j02NDPROTO=cGen2NDPROTO.genjacobian();

 %generate symbolic jacobian matrix

%Calculation of rank and size of Jacobian matrix

rank(j02NDPROTO)

size(j02NDPROTO)

%calculating numerically the rank of the Jacobian matrix by cycling through selection
of angles of joints j1, j2 and j3 using the following command

rank=rank(R2NDPROTO.jacob0([j1,j2,j3,0,0,0]));
```

ACTA UNIVERSITATIS LAPPEENRANTAENSIS

484. VUORENMAA, MARKKU. Osaamisen johtaminen pk-yrityksen kansainvälisen kasvun elinkaarella. 2012. Diss.

485. RAUTIAINEN, MARITA. Dynamic ownership in family business systems – a portfolio business approach. 2012. Diss.

486. LILIUS, REIJO. THE FINNISH IT INDUSTRIES IN TRANSITION Defining and measuring the Finnish software product and IT services industries by applying theoretical frameworks . 2012. Diss.

487. TUOMINEN, PASI. The purpose of consumer co-operation: implications for the management and governance of co-operatives. 2012. Diss.

488. SAARI, ESA. Suurnopeus-turbokoneroottoreiden termodynaaminen ja mekaaninen mallinnus sekä rakenneanalyysi. 2012. Diss.

489. PAANANEN, MIKKO. On innovative search: the use of internal and external sources of innovation among Finnish innovators. 2012. Diss.

490. BELOVA, POLINA. Quasiclassical approach to the vortex state in iron-based superconductors. 2012. Diss.

491. HIETANEN, IIRO. Design and characterization of large area position sensitive radiation detectors. 2012. Diss.

492. PÄSSILÄ, ANNE. A reflexive model of research-based theatre Processing innovation of the cross-road of theatre, reflection and practice-based innovation activities. 2012. Diss.

493. RIIPINEN, TOMI. Modeling and control of the power conversion unit in a solid oxide fuel cell environment. 2012. Diss.

494. RANTALAINEN, TUOMAS. Simulation of structural stress history based on dynamic analysis. 2012. Diss.

495. SALMIMIES, RIINA. Acidic dissolution of iron oxides and regeneration of a ceramic filter medium. 2012. Diss.

496. VAUTERIN, JOHANNA JULIA. The demand for global student talent: Capitalizing on the value of university-industry collaboration. 2012. Diss.

497. RILLA, MARKO. Design of salient pole PM synchronous machines for a vehicle traction application. 2012. Diss.

498. FEDOROVA, ELENA. Interdependence of emerging Eastern European stock markets. 2012. Diss.

499. SHAH, SRUJAL. Analysis and validation of space averaged drag model for numerical simulations of gas-solid flows in fluidized beds. 2012. Diss.

500. WANG, YONGBO. Novel methods for error modeling and parameter identification of redundant hybrid serial-parallel robot. 2012. Diss.

501. MAXIMOV, ALEXANDER. Theoretical analysis and numerical simulation of spectral radiative properties of combustion gases in oxy/air-fired combustion systems. 2012. Diss.

502. KUTVONEN, ANTERO. Strategic external deployment of intellectual assets. 2012. Diss.

503. VÄISÄNEN, VESA. Performance and scalability of isolated DC-DC converter topologies in low voltage, high current applications. 2012. Diss.

504. IKONEN, MIKA. Power cycling lifetime estimation of IGBT power modules based on chip temperature modeling. 2012. Diss.

505. LEIVO, TIMO. Pricing anomalies in the Finnish stock market. 2012. Diss.

506. NISKANEN, ANTTI. Landfill gas management as engineered landfills – Estimation and mitigation of environmental aspects. 2012. Diss.

507. QIU, FENG. Surface transformation hardening of carbon steel with high power fiber laser. 2012. Diss.

508. SMIRNOV, ALEXANDER. AMB system for high-speed motors using automatic commissioning. 2012. Diss.

509. ESKELINEN, HARRI, ed. Advanced approaches to analytical and systematic DFMA analysis. 2013.

510. RYYNÄNEN, HARRI. From network pictures to network insight in solution business – the role of internal communication. 2013. Diss.

511. JÄRVI, KATI. Ecosystem architecture design: endogenous and exogenous structural properties. 2013. Diss.

512. PIILI, HEIDI. Characterisation of laser beam and paper material interaction. 2013. Diss.

513. MONTO, SARI. Towards inter-organizational working capital management. 2013. Diss.

514. PIRINEN, MARKKU. The effects of welding heat input usability of high strength steels in welded structures. 2013. Diss.

515. SARKKINEN, MINNA. Strategic innovation management based on three dimensions diagnosing innovation development needs in a peripheral region. 2013. Diss.

516. MAGLYAS, ANDREY. Overcoming the complexity of software product management. 2013. Diss.

517. MOISIO, SAMI. A soft contact collision method for real-time simulation of triangularized geometries in multibody dynamics. 2013. Diss.

518. IMMONEN, PAULA. Energy efficiency of a diesel-electric mobile working machine. 2013. Diss.

519. ELORANTA, LEENA. Innovation in a non-formal adult education organisation – multi-case study in four education centres. 2013. Diss.

520. ZAKHARCHUK, IVAN. Manifestation of the pairing symmetry in the vortex core structure in iron-based superconductors. 2013. Diss.

521. KÄÄRIÄINEN, MARJA-LEENA. Atomic layer deposited titanium and zinc oxides; structure and doping effects on their photoactivity, photocatalytic activity and bioactivity. 2013. Diss.

522. KURONEN, JUHANI. Jatkuvan äänitehojakautuman algoritmi pitkien käytävien äänikenttien mallintamiseen. 2013. Diss.

523. HÄMÄLÄINEN, HENRY. Identification of some additional loss components in high-power low-voltage permanent magnet generators. 2013. Diss.

524. SÄRKKÄ, HEIKKI. Electro-oxidation treatment of pulp and paper mill circulating waters and wastewaters. 2013. Diss.